Contribution to the study of water resources in the coastal region of Essaouira, using vertical electrical soundings, electrical resistivity tomography and GIS (Essaouira, Morocco)

Zakaria Ouzerbane (ouzerbanegeophy@gmail.com)
Moulay Ismail University
Ali Essahlaoui
Moulay Ismail University
Abdellah El Hmaidi
Moulay Ismail University
Abdelhadi El Ouali
Moulay Ismail University
Abdessamad Najine
Université Sultan Moulay Slimane

Research Article

Keywords: Electrical sounding, Electrical tomography, Aquifers, Groundwater, Essaouira plain, Turonian

Posted Date: September 22nd, 2022

DOI: https://doi.org/10.21203/rs.3.rs-2076553/v1

Abstract

The geophysical study using the VES and the ERT, carried out in the coastal area of Essaouira (Morocco), for the purpose of mapping the aquifers by combining the two geo-electrical methods, the results allowed us to determine the lateral and vertical distribution of the geological formations in the study region. Thereafter the exploitation of these results by the decision makers in the choice of the sites likely to be hydrogeologically fertile to answer the need for the inhabitants in resource in water. The synthesis on the evolution of the geological layers, the variations of thickness and to highlight the anomalies which could affect them, the GIS tool makes it possible to draw up maps (VES) and electrical imagery (ERT) at a depth chosen by data interpolated by Kriging. The analysis of the results shows that the Qsob zone is of paramount hydrogeological interest, it is represented by a very important layer given the great extension of the resistant formations of Plio-Plioctecene and Cretaceous age with significant thicknesses. The area is crossed by the Qsob River which is the main source of supply for these two aquifers. With the communication of the two aquifers by the very abundant and dense electric discontinuities of general directions E-W, NE-SW and NNE-SSW.

1. Introduction

Morocco is one of the Mediterranean countries currently experiencing intense demographic, social, cultural, economic and environmental changes. Water resources in the countries around the Mediterranean are limited and unequal. The Mediterranean bassin regroups 60% of the water-poor world population with water capital/inhabitants less than 1000 m^3/inhabitant/year, in Morocco, it is less than 650 m^3/inhab/year (Sinan et al., 2009 ; Ouzerbane et al, 2021a). Resources are already overexploited in many places and the growth in water needs will remain very strong with population growth in the southern Mediterranean basin, the development of tourism, industry and irrigated land. The scarcity of water resources in the Kingdom is not an exceptional concept. It stems from the peculiarities of the geographical and climatic context of the region. The various processes, cited above, will exacerbate the problems of availability of this resource in quantity and quality. This will accentuate the tension between supply and demand (Calow et al., 2010 ; Jamaa et al., 2020). Such situations will recur in the future and perhaps even more frequently if they are linked to the phenomenon of desertification which affects West Africa and to the extent of climate change on a planetary scale. This water crisis is aggravated by the dynamic interaction of several processes that act at the local, national and global level (Bahir et al, 2002, Ouzerbane et al, 2021b). Globally, the total volume of groundwater resources is difficult to measure, but one estimate puts it at around 10.5 million km³ (Shiklomanov and Rodda, 2003), with groundwater resources remaining the main source of water fresh water on Earth, with more than 90% of fresh water immediately available (PNUE, 2008; Boswinkel, 2000). Aquifers are increasingly in demand, as modern capture technologies are becoming widespread, while surface water resources, which are more accessible, are gradually being overexploited with 50% for domestic use; 40% in industry; and 20% in irrigation water supply (Zektser and Everett, 2004). Groundwater is essential for securing water supplies

in arid and semi-arid regions and is a factor of resilience in the face of climate change (Bahir et al., 2001 ; Karroum et al., 2017 ; Ouhamdouch al., 2019).

Faced with these problems, it's necessary to put in place mechanisms and actions aimed at recognizing, preserving and safeguarding water resources. The study area is represented by the coastal part of the Essaouira basin which is part of the Moroccan Atlantic coast with an arid to semi-arid climate. It's a space that is given a heavy responsibility in the socio-economic development of Morocco (Chamchati et al., 2013 ; Ouzerbane et al., 2014; Ouhamdouch et al., 2016b ; Bahir et al., 2019 ; Jamaa et al., 2020). This development implies a significant increase in water needs in the years to come, both for drinking water supply and for irrigation and industry (Ouhamdouch et al., 2018b ; Chafouq et al., 2018 ; Jamaa et al., 2020). The Essaouira basin has experienced, like other regions of Morocco, a significant decrease in water inflows in quantity and quality. This situation has led to a reduction in agricultural productivity and the degradation of several ecosystems. However, this basin has an aquifer system made up of a set of aquifers of unequal importance. These aquifers can provide a natural regulating capacity that makes them valuable for safely ensuring a steady supply. The reserve also makes it possible to meet seasonal needs thanks to temporary overexploitation insofar as reconstitution is possible. The overexploitation of aquifers, especially in arid and semi-arid regions, leads to environmental problems, an increase in pumping costs and above all the depletion of the resource for future generations (Urish and Frohlich, 1990; Sherif et al., 2006; Attwa and Zamzam, 2020 ; Shah et al, 2007 ; Ouzerbane et al, 2021c). Water quality is essential for the well-being of the inhabitants of the coastal zone of Essaouira, the maintenance of healthy aquatic ecosystems and the activities of the primary sector, in particular agriculture, tourism and aquaculture. Quality problems rendering water unusable only exacerbate scarcity (e.g., Calow et al., 2010; Ouzerbane et al., 2014 ; Manu et al., 2016 ; Ouhamdouch et al., 2016a). With an increasing demand for water and an often insufficient resource, the Tenssift hydraulic basin agency (ABHT) and the National Office for Drinking Water and Electricity (ONEE) still favor the development of supply. So, the exploitation of groundwater, hydraulic developments and the use of non-conventional water are the means implemented to meet drinking water needs, particularly for agriculture. The integrated and participatory management of water resources and demands has been selected as the first area of action for decision-makers in the province of Essaouira, with water demand management issues of a different nature, in some places, the qualitative aspects of the resource prevail, as well as the interest in maintaining, or even restoring, ecosystems, thereby lowering the cost of water supply (Ouarani et al., 2021 ; Ouzerbane et al., 2021a). The coastal zone of Essaouira is tightening between a limited water resource and strongly increasing demands, the challenge is still above all quantitative. It is fundamental not only to consider water as a resource, but also to understand its importance for the functioning of complex ecological systems (Chamchati et al., 2013 ; Ouzerbane et al., 2019 ; Ouarani et al., 2020; Ouzerbane et al., 2021a; Ouzerbane et al., 2021b).

Local solutions, based on field knowledge, are necessary for the sustainable integrated management and protection of ecosystems. In this context, the geophysical study presented here aims to define the geometric characteristics of the superficial aquifer (Eluwole et al., 2018), in order to better understand the geological structure and plan the judicious location of groundwater exploitation boreholes (Souid, 1983;

Medina, 1994; Piqué, 1994; Broughton and Trépanier, 1993; Piqué and Laville, 1996 ; Piqué et al., 1998 ; Hafid, 2000; Mader et al., 2017). The study by electrical soundings (VES) and electrical tomography (ERT), as well as hydrogeological mapping, and the collection of agricultural and socio-economic data are all data that must be integrated in digital form to obtain land classification maps that can be easily used by developers and planners in the Marrakech-Safi region and to plan the judicious location of groundwater exploitation boreholes (e.g., Bhattacharya and Patra, 1968 ; Bose and Ramkrishna, 1978; Urish and Frohlich, 1990; Devi et al., 2001; Sainato et al.,, 2003; Owen et al., 2005; Sharma and Baranwal, 2005; Singh et al., 2005; Yadav and Singh, 2007; Francese et al. 2009; Kumar et al., 2010, 2014; Chandra et al., 2012; Ebraheem et al., 2012; Zaidi and Kassem, 2012; Anechana et al., 2015; Manu et al., 2016; Sikah et al., 2016 ; Himi et al., 2017 ; Essahlaoui et al., 2003 ; Wafiq et al., 2019). In this regard, the use of a geographic information system (GIS) is necessary. The geological information collected also made it possible to facilitate the choice of geophysical methods best suited to the context of the study and to better implement the geophysical measurement grids (Ouzerbane et al., 2018b).

2. Geographical Location Of The Study Area

The Essaouira basin is a coastal area located in the center-west of Morocco. It belongs to the Moroccan Atlantic margin and covers approximately an area of 20000 km² of the Eastern Mesozoic Passive Margin of the Central Atlantic Ocean. The basin is bounded to the north by the Tensift river, to the south by the Western High Atlas, to the east by the plains of Imi-N-Tanoute and Chichaoua and to the west by the Atlantic Ocean. It is a plateau, slightly raised to the south and north, gently sloping down towards the Atlantic Ocean then dropping sharply to give rise to the coastal zone with dune relief.

The Essaouira syncline study area is part of the coastal zone of the Essaouira basin with an area of approximately 1418 km^2 (Ouzerbane et al., 2018a). It is bounded to the north by Jbeb Hadid, to the south by Tidzi river, to the east by the reliefs of Chiadma south and Haha north and by the diapir of Tidzi and to the west by the Atlantic Ocean. It is not very rugged and is characterized by a relief of low hills with altitudes between 0 and 800 meters, shaped by a low-density hydrographic network that flows into the Atlantic Ocean (Fig. 1).

3. Geological Situation Of The Study Area

The Essaouira basin has two tectono-stratigraphic series (Fig. 2) :

A synrift series of Lower Triassic-Liassic age, emplaced above a Paleozoic bedrock structured by the Hercynian orogeny ; this Triasico-liasic series is formed mainly by lacustrine, fluvio-deltaic to marine detrital deposits, evaporitic deposits and basaltic flows ;

A post-rift series of Upper Liassic-Eocene age, formed by proximal platform deposits in general (Ouzerbane, 2015 ; Ouzerbane et al., 2019 ; Cohen et al., 2020).

From the structural point of view, the basin is part of the North Atlas furrow defined by Ambroggi (1963) as being a zone of moderate folding. The structure of the basin is represented by a succession of anticlines and synclines which resulted from the combination of the effects of Atlas tectonics and diapirism. The whole of the basin is fragmented by major accidents which extend under the cover and which are inherited from the Hercynian tectonic phase (Souid, 1983; Medina, 1994).

3.1 Paleozoic (ante-rift deposits)

It is known at the outcrop in the circumference of the basin at the level of the Jebilets and the Western High Atlas and by drilling in the center of the basin.

The Cambrian : It exists on the eastern edge of the basin resting unconformably on the Precambrian basement. It is formed by argillaceous quartzitic sandstones surmounted by compact quartzites.

The Ordovician : Represented by epicontinental terrigenous deposits, transgressive on the Cambrian deposits.

The Silurian : it is formed by gray silty clays with rare intercalations of grey-beige limestone.

The Devonian : Includes argillaceous limestones, grey-brown limestones and silty red clays presenting past fine sandstones and marls.

The Carboniferous : The deposits of this system have never been reported in the Essaouira basin.

The Permian : Made up of conglomeratic deposits to the north of the Doukkala basin (Machraa Ben Abou) and in the Argana corridor.

3.2 Mesozoic and Cenozoic

3.2.1 Triassic age

In the Essaouira basin, synrift deposits outcrop only at the level of the Tidsi diapir in the form of red saliferous clays and shreds of basaltic flows called "ophites" (Suter, 1958) in the north of Jbel Kourati. In the subsurface the synrift series overlies unconformable Paleozoic deposits. It presents from bottom to top the lower salt, clay, sandstone and conglomerates, followed by the basalt, then the post-basaltic Triassic formed by siltstones, clays and salts. The Triasico-liasic formations are surmounted by epicontinental carbonated marine deposits (Fig. 2).

3.2.2 Jurassic age

Middle-Upper Lias : It is formed by oncholite limestone constituting the Arich Ouzla Formation which outcrops in the Jbel Amsitten region. The Domerian is formed by a fluvio-deltaic regressive detrital series corresponding to the Amsitten Formation (Fig. 2).

Toarcian-Lower Aalenian : The Toarcian-Aalenian is formed by limestone and dolomites, marls and gypsum.

Upper Aalenian-Bathonian : It is formed by silico-clastic detrital deposits and whose lateral equivalent.

Callovian-Middle Oxfordian : It corresponds to marl-limestone deposits. It constitutes the Sidi Rhalem formation dated by ammonites (Roch, 1931).

Upper Oxfordian : It is represented by lithographic limestones with fine bedding emplaced in a confined environment. The deposits correspond to the Hadid Formation (Medina, 1994; Piqué, 1994).

Lower Kimmeridgian : During the Lower Kimmeridgian there is a sudden change in the sedimentation regime with the establishment of evaporitic and sometimes detrital deposits.

Upper Kimmeridgian - Portlandian / Berriasian : They are represented by carbonates, essentially dolomites and evaporites (anhydrites and gypsum). The base of this set is dated to the Upper Kimmeridgian, while at the top the Calpionelles associations do not make it possible to separate the Portlandian from the Berriasian (Taj-Eddine, 1991).

3.2.3 Lower Cretaceous age

It is characterized by an essentially marine regime with neritic limestones and marls alternating with episodes with red silico-clastic deposits (Fig. 2).

Upper Berriasian-Basal Valanginian : It includes more or less silty marl limestones and fossiliferous marls.

Lower Hauterivian : Consisting of marl deposits interspersed with a few limestone and sandstone beds evolving towards channel deposits or towards madreporary reef limestones.

Upper Hauterivian : Consisting of marls and red sandstone passing eastward to red and green clays with intercalations of sandstone limestone with oysters, presenting horizontal or intersecting stratifications (Duffaud et al, 1966 ; Rey et al, 1950).

The Barremian : Represented by marly grey-green limestones, sometimes lumachelic.

The Aptian and Albian : Comprising conglomeratic sandstones, marls and marly limestones with ammonites, the Tadhart Formation consisting of limestones with ammonites and marl intercalations ; the Tidsi river Formation is made up of marly limestone with pyritic ammonites and sandstone limestone (Rey et al, 1950).

3.2.4 Upper Cretaceous age

The Cenomanian is represented by marls, limestones and dolomites corresponding to the Aït Lamine Formation and representing a general transgression to the entire basin (Choubert and Faure-Muret, 1962).

The Turonian corresponds to marl-limestone and dolomitic limestone with anoxic clayey levels corresponding to the black shales recognized throughout the world.

The Coniacian-Santonian is represented by dolomitic limestones, dolomites and gypsiferous red marls.

The Campanian corresponds to a detrital and evaporitic episode with gypsiferous and sandstone-dolomitic red marls.

The Maastrichian is represented at the base by a bar of silicified limestone followed by a marl-dolomitic series (Choubert and Faure-Muret, 1956 ; Duffaud, 1970a).

3.2.5 Tertiary age

Represented by Marly deposits of Montien and phosphate sands with Odontaspis macrota and Myliobatis ; Marl and marl-limestone from the Lower Eocene ; Limestones, marls, and oyster-bearing marl-limestones and nautiluses dating from the Middle Eocene (Lutetian) ; Sands, sandstones and red marls dating from the Upper Eocene ; White conglomerates found at Imi n'Tanout and dated to the Oligocene (Fig. 2).

3.3 Plio-Pleistocene and Quaternary

The lithostratigraphy of Plio-Pleistocene deposits shows the succession of several depositional environments (marine, littoral, fluvial, and lacustrine), separated by discontinuities (Fig. 2).

The organization of these deposits in sedimentary filling sequences is related to the geodynamic evolution of the basin. The situation of the Quaternary marine deposits below the Moghrebian deposits, and their arrangement in stepped systems, within which are nested continental deposits, evoking successive withdrawals from the sea.

Overall, it can be seen that the palaeographic evolution of the Essaouira region, during the Plio-Pleistocene, was controlled on the one hand by the combined effects of sea level fluctuations, tectonic uplift behind country and on the other hand by local climatic modifications. The latter played a determining role in the variation of the nature of the sedimentary contributions and in the installation of certain deposits (Barkhanes). The diagenetic study of Plio-Pleistocene coastal marine deposits shows that they have undergone diagenetic processes characterized by early and late cementations which depend on the hydrodynamic conditions of the deposit environment and the geodynamic evolution of the entire basin. Some of these Plio-Pleistocene deposits have calcareous crusts at their summits, often surmounted by zonal crusts with lamellar structures. The study of these calcareous crusts has allowed the observation of interference and alternation of several important stages in the history of their formation (sedimentological, biological and diagenetic), in relation to climatic variations (humidity, drought).

4. Hydrogeological Context Of The Study Area

4.1 Plio-Pleistocene aquifer

The Plio-Pleistocene in the study area is a matrix reservoir consisting of sandstone dunes and shell limestone; it extends along the Atlantic coast on a strip of 20 km wide and 30 km long. According to mechanical soundings and reconnaissance wells carried out in the area by the Tenssift Watershed Agency, the reservoir is productive only when it is in perched position resting on the impervious marls of the Cretaceous or Jurassic, where the Plio-Pleistocene rests directly on the permeable formations; the water infiltrates vertically to feed the deep aquifer. The saturated thickness of the aquifer varies from 10 to 60 m and extracted flows do not exceed 10 l/s (Mennani, 2001). The feeding of the groundwater is carried out on the one hand by the infiltration of the rainwater and on the other hand by the infiltration along the rivers, with a general flow of the aquifer which is carried out towards the ocean it is due to the dipping of Cretaceous formations towards the West. The reservoir has a transmissivity with a large dispersion; it varies from 6 10^{-2} to 4.5 10^{-5} m^2/s (Mennani, 2001 ; Ouhamdouch et al., 2018).

4.2 Cretaceous aquifer

It is the most important aquifer due to its extension and its hydrodynamic characteristics, its properties are related to the existence of discontinuities represented by stratification plans (which give rise to sources), by fracturing and also by the development of phenomenon of Karstification. It includes the dolomitic and yellow dolomite limestones of the Santonian whose thickness can reach 100 m, cracked and karstified limestones of the Turonian with a thickness of 40 to 80 m, the lumachellic limestones of the Cenomanian and gray marl-limestones with gypseous traces, fractured fossiliferous limestones and Barremian-Aptian sandstones.

Depending on the geometry and lithology of the subsoil of the study area, the Cretaceous reservoir may be free or captive, and in the absence of a significant impervious layer between the different levels gives it the character of a multilayer system where the Turonian aquifer is the most important with a transmissivity varying between 2.10^{-4} and 9.10^{-3} m^2 / s (Mennani, 2001). The Cretaceous reservoir is fed mainly from the rains and along the Igrounzar river to the south of Meskala and downstream to the south of Essaouira and possibly from the overlying plio-quaternary aquifer. The aquifer is drained by springs emerging along the Rivers Igrounzar and Qsob. The general flow of the aquifer is towards the North and the NW before reaching the Atlantic Ocean.

5. Materials And Methods

5.1 Geophysical prospecting

The geophysical study carried out in the coastal area of Essaouira began with a geological reconnaissance of the area to be prospected. During this initial phase, this reconnaissance consisted of obtaining all the information relating to the characteristics of the soil and the subsoil. Indeed, the geological study has made it possible to better identify the type of rock or material, the structure of the

different formations, the sedimentological environment, the mode of formation or genesis of the different facies and also to identify the state of weathering and fracturing (Fon et al., 2012; Fuh et al., 2019; Mashhad et al., 2020 ; Asfahani, 2016; Bersi and Saibi, 2020 ; Perrone et al., 2004; Sajinkumar et al., 2015 ; Sherif et al., 2006 ; Ogungbe et al., 2012 ; Akintorinwa and Abiola, 2011 ; Arisona et al., 2020). This collected geological information makes it possible to establish correlations with hydrological, lithological and petrographic information and also to facilitate the choice of the measurement devices most suited to the study context and to better implement the data acquisition profiles (Flathe, 1955; Ghosh, 1971; Kosinky and Kelly, 1981; Mazac et al., 1985; Yadav and Abolfazli, 1998; Hodlur et al., 2006 ; Asfahani, 2016 ; El Bouhaddioui et al., 2016).

In parallel with this phase of the study, all the data relating to the hydrogeology of the study area was collected. These data were collected through a campaign of piezometric surveys and lithologic identification of aquifer levels.

At the end of this campaign, a work of analysis of all the information was carried out. The data was accommodated, analyzed and then integrated into a preliminary database which was updated as the work progressed. The data acquisition was followed by the establishment of geoelectric sections on which the layers are indicated with their resistivities, thicknesses and depths.

In view of the limitation of vertical electrical soundings (VES) to the determination of lateral variations of the electrical resistivity of the subsoil (Store et al., 2000 ; Okrah et al., 2012 ; Radouani et al., 2013), the method of electrical resistivity tomography (ERT) is developed with the aim of obtaining a subsoil model whose resistivity distribution varies vertically and horizontally along the profiles, this variation is a function of many intrinsic properties of the soil such as its mineralization, grain arrangement, porosity, material density, compaction, temperature and subsoil water content (Russel and Barker, 2010). The apparent electrical resistivities are then inverted to obtain an interpreted resistivity model (Reynolds, 1997).

The equipment used for the vertical electrical soundings is a Syscal R1 Plus resistivity meter specially designed for prospecting superficial and underground terrains, it is perfectly suited to hydrogeological and structural studies (Sharma, 1997). It can be used to study variations in resistivity as a function of depth (electrical soundings) as well as lateral variations in resistivity along a profile (electrical trails). The Syscal R1 resistivity meter is designed to work with different types of devices such as Schlumberger, Wenner, dipole-dipole, pole-dipole, and pole-pole.

5.2 GIS and Choice of spacing and depth of investigation for ERT

We use the GIS and from the data resulting from the interpolation by kriging of the electrical soundings carried out in the coastal region of Essaouira at different prospected levels, we have produced pseudo-sections, which qualitatively reflect the spatial and vertical variation of the apparent resistivity, so minimize the error of Schlumberger (VES) and Schlumberger-Wenner (ERT) device investigation depth

ratio by choice of inter-electrode spacing (Loke, 2010). This kriging interpolation method is an interpolation that estimates the values at non-sampled points by a combination of data. The weighting of the points is performed by a structure function derived from the data. It is therefore taken into account distances, values and correlations. It is a technique for calculating moving averages using the parameters of a variogram to obtain a good estimate of the relationship between data points. The latter corresponds to the evolution of the semi-variance as a function of the lag between the points.

In practice, the inversion is applied to the VES kriging data with a spacing of 40 m (Table 1). The location of the tomography profiles is chosen in a way that more or less coincides with the location of the profiles of the VESs already made (Fig. 3, 4). In this case, it is assumed that the resistivity does not change in the direction perpendicular to the profile.

Table 1
Investigation depth of the device used with a = 40 m (Loke, 2010). Z_{s-w}: ERT Investigation Depth. L: Length of tomographic profile. AB: Length of SEV Profile. Z_s: SEV Investigation Depth.

Schlumberger – Wenner (ERT)				**Schlumberger (VES)**			**Error**
n	L= (2n + 1)a	Z_{s-w}/L	Z_{s-w}	AB	Z_s/AB	Z_s	$(Z_s-Z_{s-w})/Z_s$
1	120	0.173	20.76	120	0.190	22.8	0.089
2	200	0.186	37.2	200	0.190	38	0.021
3	280	0.189	52.92	240	0.190	45.6	0.138
4	360	0.190	68.4	300	0.190	57	0.167
5	440	0.190	83.6	400	0.190	76	0.091
6	520	0.190	99.32	500	0.190	95	0.043
7	600	0.190	114.6	600	0.190	114	0.005
8	680	0.190	129.88	-	0.190	-	-
9	760	0.190	145.16	800	0.190	152	0.045
10	840	0.190	160.44	-	-	-	-
11	920	0.190	175.72	-	-	-	-
12	1000	0.190	191	1000	0.190	190	0.005

5.3 Inversion of electrical sounding data (VES) for tomography (ERT).

To obtain the real soil resistivity at the level of the profiles, the apparent resistivity values must be inverted. The principle of inversion consists in determining underground models (interpreted resistivity)

whose electrical response reproduces the measured apparent resistivities (pseudo-section).

The objective of the inversion is to determine the resistivity distribution which minimizes the difference between the pseudo-section calculated for a subsoil model and the measured pseudo-section. This difference is generally quantified by the least squares criterion (Root Mean Square, RMS). The subsoil model obtained at the end of the inversion constitutes an approach which is not unique to represent the resistivity of the subsoil, but with the knowledge of the local geology makes it possible to retain the most representative model.

Using the Res2dinv software (Loke and Barker 1996), the data measured on the ground are inverted. It is the most widely used tool in electrical resistivity tomography (ERT) applications.

By default, the software first generates an initial model of the subsoil with a homogeneous resistivity composed of layers of increasing thickness with depth. This initial homogeneous resistivity is calculated at each measurement point according to the acquisition parameters used when taking the measurements. The thickness of the first layer is determined by default according to the device used and the inter-electrode spacing. The thicknesses of the other layers increase with the depth according to the choice of the user. Each layer is made up of a number of rectangular cells. From the information included in the measurement file (in particular the type of measurement device and the inter-electrode spacing), the program calculates the response of the model in apparent resistivity (ρ_{cal}) at the measurement positions. The Res2dinv software then seeks to reduce the difference between the calculated values and the measured values (ρ_{mes}) by modifying the resistivities of the model. The reduction of this difference is done in the sense of least squares using an iterative process. The resistivity of each cell of the model is thus updated after each iteration. When the difference between the measured and calculated pseudo-sections no longer changes significantly, the program stops the inversion process by presenting the RMS which provides some information on the mathematical reliability of the determined subsoil model (Loke and Barker 1996).

6. Results And Discussion

6.1 Qualitative and quantitative interpretation of VES results

The results of the geo-electrical study carried out in the coastal zone of Essaouira, led to the establishment of certain apparent resistivity. From these qualitative maps one can derive ideas and information on the lateral variations of the resistivity of a given region for different slices of land corresponding to different spacings of the electrodes AB of injection of electric current (eg, Atzemoglou and Tsourlos, 2012; Essahlaoui et al., 2001; Geoscan-M Ltd., 2001).

This geo-electrical study (SEV) has led us to relevant results (Ouzerbane et al, 2013 ; Ouzerbane et al, 2014 ; Ouzerbane et al, 2021a), is the subject of certain research work by Ouzerbane et al. and from the

maps of the apparent resistivities of the research work, the data of the Tomography (ERT) have been resourced.

6.1.1 Apparent resistivity map for AB = 160 m

Establishing the map of apparent resistivities for the length of line chosen (AB = 160 m) makes it possible to characterize flush or sub-flush deposits (Fig. 5).

The analysis of this map shows a lateral variation in resistivity, with conductive zones located to the east of the study area (Ounara-Had Draa region) and in the center between Qsob river and Tidzi river. These conductive zones may correspond to marl and marl-limestone of the Cretaceous age with a resistivity varying between 44 and 77 Ohm.m, where the Plio-Pleistocene outcrops are very small (Ouzerbane et al., 2013 ; Ouzerbane et al., 2021a).

Resistant zones with resistivities greater than 77 Ohm.m covering the majority of the study area and whose maximum is around 320 Ohm.m in the North-East especially in the North of Oued Qsob. In correlation with the mechanical drillings and the geological maps, these zones being able to be correlated with the sandstones, Sands and alluviums of Quaternary and Plio-Quaternary age except in the South of the Tidzi wadi where the distribution of the apparent resistivity given by this length AB = 160m, may correspond to limestone with Flint and marly limestone of Barremo-Aptian age (98–120 Ohm.m).

6.1.2 Map of apparent resistivities for AB = 500 m

When the AB current injection line is increased, the effects of sub-outcropping terrain become negligible (Dey and Morrison, 1979; Zhody, 1989; Gupta et al., 1997; Yadav et al., 1997; Basokur, 1999; Singh et al., 2005, 2013; Piatti et al., 2010; Srinivas et al., 2012; Essahlaoui, 2000; Essahlaoui et al., 2001, Essahlaoui and El Ouali, 2003 ; Alfaifi et al., 2019).

Examination of the apparent resistivity map (Fig. 6) obtained shows an increase in resistivity from the South to the North-West of the study area. Similarly, from the North-East to the West, the values of the apparent resistivity measured vary from 46 to 135 Ohm.m, the increase in resistivity is due to the deepening, from the North-West to the South and from the West to northeast, resistant formations of Cretaceous age, this deepening becomes important south of Qsob river (Fig. 6).

According to the analysis of the map of apparent resistivities for the length AB = 500 m, a resistant zone stands out in the North-West of the study area and corresponds to the limestones and marly limestones of the Cretaceous (lower and upper). With an apparent resistivity varying from 81 to 135 Ohm.m, the maximum resistivity is recorded in the North-West of the study area by electrical soundings SE15-21 and SE33.

This resistant zone separates the two other conductive zones located to the North-East and South (South of Qsob river) of the study area, with resistivities of 46 to 67 Ohm.m and corresponding to marl and marl-

limestone Cretaceous (lower and upper).

6.1.3 Map of the total longitudinal conductance (LC) of the Cretaceous conductor

Analysis of the map of the total longitudinal conductance obtained from the conductor data of each electrical sounding shows values vary from 0 to 7 Ohm^{-1}, zero or low values may correspond to marl and/or marl-limestone low or zero thickness and the maximum values probably correspond to marls and/or marl-limestones that are both thick and conductive. The spatial distribution of the longitudinal conductance values subdivides the study area into two well-defined zones separated by the Qsob river (Fig. 7).

An area in the North where the longitudinal conductance values increase from West to North-East of the study area, with higher values observed in the North-East of the Ounara – Had Draa area where the filling marly is important. South of Qsob river, the longitudinal conductance values increase from South-East to West where the maximum values are observed in the Sidi Kawki region and along Qsob river.

The superposition of this map (Fig. 7) with that of the apparent resistivity of the length AB = 500 m (Fig. 6) shows a certain similarity. Certainly, the zones having low longitudinal conductance are characterized by the strongest apparent resistivities, and contrary, the zones with high values of longitudinal conductance coincide with the zones with low values of the apparent resistivities.

The longitudinal conductance map and that of the apparent resistivities AB = 500 m are very important, they can more reliably give the appearance of the roof of the resistant Cretaceous age (limestone, sandstone and marly limestone).

6.1.4 Map of the total transverse resistance (TR) of the Cretaceous resistant

The map of the total transverse resistance (Fig. 8) is obtained by the geometric and physical data at the right of each electrical sounding, this map shows the values of the transverse resistances ranging from 5116 to 21964 Ohm.m2, with the largest values observed to the east of the study area, especially around electrical boreholes SE39, SE45 and SE54.

The high values of the transverse resistance indicate that either the thickness of the formation is large or the resistivities which are very high or both at the same time, which is observed around borehole SE45. One notices around the zones where the values of TR are very high, the transverse isoresistant curves are very tight and materialize a strong gradient shows the rise of the resistant of Cretaceous age (upper and lower) which plunges towards the Atlantic Ocean where it gets deeper and deeper.

The superposition of both the map of the total transverse resistance (Fig. 8) with that of the total longitudinal conductance (Fig. 7), shows the different zones of contact and probable direct

communication between the two aquifers (Plio-Pleistocene and Cretaceous) from the hydrogeological point of view.

6.1.5 Map of the isohypses of the roof of the Cretaceous resistant

The map of the isohypses of the roof of the resistant Cretaceous age (lower and/or upper) gives the structure of the coastal zone of the Essaouira basin (Ouzerbane et al., 2021a). It defines the behavior of the resistant grounds which represent the deep aquifer of this zone, it is a multilayer system sometimes captive or/and semi-captive and sometimes free (Fekri, 1993). This map of the isohypses highlights the dip of the resistor generally towards the West of the study area, with a general direction from the South-East to the West and towards the North-West (Fig. 9).

The Qsob North Zone (South Chiadma), it is located north of Qsob river, in this area the resistant plunges from South-East to North-West, this depression is done by a weak dip. The resistant is very spread out towards the North and the North-West where it is attributed to massive limestones of Vraconian age with an average depth, on the other hand it is attributed to limestones and marly limestones of Cenomanian in the South-East and East where the resistant is flush and/or sub-flush (Fig. 9). But the Qsob South Zone (North Haha), it is located south of Qsob river, in this zone the resistant dip is from East to West and from South-East to North-West with a very steep dip. The Cretaceous age resistance is located at the highest depths on the scale of the studied area, where the thickness of the marl formations can exceed 150 m or even more (SM362/51 and SE40-42). It forms a zone around the Qsob river with closed and very tight isohypse curves (Fig. 9).

6.2 Interpretation of ERT results

The first step in the interpretation of electrical tomography (ERT) data was performed using the inversion method of Loke and Barker (1996). The effectiveness of this modeling method has been widely proven in multiple cases of geophysical prospecting study applied to geological reconnaissance and structural mapping of deep and superficial underground aquifers. This method was systematically applied to all the tomography profiles implanted at the level of the study area (Fig. 4) in an East-West direction. This allowed us to obtain models of the subsoil in the form of a section of the real resistivity of the investigated terrains.

The fine analysis of the pseudo-sections makes it possible to realize the significant variations of the intrinsic resistivity thus testifying to the fragmented character of the geological structures and the remarkable influence of the paleogeography (environments of different deposits, transgression, regression, etc.).

The results of the geophysical survey (Fig. 3) show measured data in the form of real resistivity models of the basement obtained by inversion of these data. A first examination of all the results obtained

reveals the existence of significant variations in the electrical resistivity of the subsoil, testifying to its heterogeneity. Schematically, the area covered by the geophysical survey is formed by 4 geoelectrical levels corresponding to 4 major lithological units:

- - A resistant level (R_1) of resistivity greater than 100 Ω.m corresponding to the karstic limestone level of the Turonian, dolomitic limestone of the Cenomanian and massive limestone of the Vraconian. This observation is justified by the first calibration surveys carried out on the surface of the Cretaceous outcrops present in the east of the coastal zone of the Essaouira basin.
- - A less conductive level (C_1) of resistivity lower than 100 Ω.m corresponding to the alternation of marl and marl-limestone from the Santonian and Cenomanian;
- - A resistant sandstone bench (R_2) well represented on the profiles, its resistivity is located beyond 250 Ω.m. This resistance has been attributed to the consolidated sandstones of the Plio-Pleistocene.
- - A very conductive level (C_2) of resistivity lower than 50 Ω.m corresponding to the quaternary alluvia located in the center of the basin and may also correspond to gray plastic marls of Cretaceous age (lower and/or upper).

6.2.1 Line 1 (South Hadid)

The subsoil resistivity model obtained along line 1 shows an important resistant zone at the extreme east of the section separated from another more conductive zone located towards the west (Fig. 10).

Given the location of this profile, it is clear that the resistant R_1 observed on the surface at the western end of the profile corresponds to the sandstone level of the Plio-Pleistocene with a low thickness. Towards a depth of about 80 m, a resistant R_2 corresponding to the Vraconian is separated from a more conductive block located to the south and shows two well-defined levels:

- - The superficial conductor C_1 located in the middle and to the east of the profile would represent the marly and marl-limestone formations of the Cenomanian age.
- - The C_2 conductor corresponding to the Barremo-Albian marl formation.

6.2.2 Line 2 (Agadir Chicht – Matrazza)

The resistivity pseudo-section obtained along this line shows two resistant masses of unequal size separated by a conductive zone C_1 which would correspond to the lower marl-limestone layer (Fig. 11). As for line 1, the resistant mass will represent the sandstone beds with a very important thickness. However, at this line, this bar appears more extensive towards the East and plunges towards the West according to the tectonic effect and the altitude of the reliefs of the natural terrain. It continues to the western end of line 2, where it stops abruptly. This suggests a northern extension of the fault also noted at line 3.

6.2.3 Line 3 (El Araich – Had Draa)

On this line, we find the rise of resistant R_2 (Vraconian) predicted by the local geology (Fig. 2) with the effect of tectonics. Thus, in addition to the superficial conductor (C_1) which should correspond to a marly and marl-limestone layer of the Cenomanian towards the east of the profile. We find the three lithological units schematized on line 2, namely the sandstone bed (resistant R_1) with a very significant thickness towards the West, the marl-limestone layer (conductor C_1) and the massive limestone (resistant R_2).

In accordance with the surface geology, the series presents a disturbance towards the East due to the presence of a series of faults and flexures already detected in the first section. The sandstone bar is continuous to the east on line 3 with a decrease in thickness. A relative drop in resistivity at this location could correspond to the southern extension of the fault mentioned above but which does not show a vertical rejection at this location (Fig. 12).

With the effect of tectonics, disturbances were detected along the profile and having the same continuity as that detected in all the profiles.

It is at the level of this region where there are reliefs and the geometry of the geological formations (superficial and deep) of higher altitudes compared to the whole of the zone studied, it shows the existence can be of an anticline which separates the South Hadid syncline and the Qsob river syncline.

6.2.4 Line 4 (El Aarabate – Ounara)

It mainly highlights the 3 aforementioned geological entities (Fig. 2). Indeed, the resistivity model obtained shows a deep resistant (R_2) which would materialize the continuity of the Turonian age layer. The latter is surmounted by a C_1 conductor which would represent the upper marl layer of the Santonian. The sudden decrease in resistivity west of line 4 and the decrease in the thickness of the resistant layer R_1 could be explained by diapiritic upwellings (Fig. 13). This observation has already been mentioned in several studies and technical reports carried out in the Essaouira basin, this diapirism is manifested by intrusions of saliferous clays (Bahir et al, 2001).

6.2.5 Line 5 (Qsob river)

The pseudo-section of line 5 (Fig. 14) presents an important resistant level, represented by the dolomitic and karstic limestones of the Turonian, which appears at a depth of 50m compared to the natural ground under a wave shape.

To the east, the conductor C1 corresponds to marl and marl-limestone from the Santonian overcomes the resistant R_2. On the other hand towards the west the resistant R_2 is directly overcome by the alternation of resistant conductor attributed to sandy clays and alluvium Qsob river of Quaternary and Plio-Pleistocene age with a thickness becomes more and more important going from the East to the West and also from the North of Qsob river to the South.

The resistant R_2 rests on the conductor C_2 corresponds to marl and marl-limestone of the Cenomanian age, which behaves like a stack of synclines and anticlines fragmented by faults of different discharges.

6.2.6 Line 6 (Cap Sim – Ait El Aouni)

It highlights the resistant R_1 of Quaternary and Plio-Pleistocene age with a significant increase in their thickness compared to line 5 (Fig. 15), it overcomes a conductive formation C_1 which can correspond to very plastic gray marls of Senonian age. It presents a very important impermeable layer at the base of the resistant R_1 which presents an underground water aquifer and the only water resource in this place given their thickness and their extension. with a dip from west to east.

6.2.7 Line 7 (Sidi Kawki - Tidzi)

On this line, we find the stratigraphic succession provided by the local geology. It made it possible to have a model which highlights a thin layer of resistant R_1 of Plio-Pleistocene age (Fig. 16), based on a less conductive formation attributed to marl-limestone of Santonian age. This model shows a deeper resistant R_2, which may correspond to the Turonian age limestones outcropping north of the Tidzi river, it rests on Cenomanian age conductive marls.

The increase in thickness of the resistant layer R_1 of Plio-Pleistocene age, going from line 5 towards line 6 and their decrease going from the latter towards line 7 along a NS direction, shows that the region between Qsob river and Tidzi river presents a syncline at the heart of Santonian age surmounted by recent formations of Quaternary and/or Plio-Pleistocene ages.

6.2.8 North-South line (Agadir Chicht - Tidzi)

This section is made in such a way as to cross as many tomographic lines as possible. The model highlighted by this line of tomography shows the succession predicted by the local geology. It shows the geometry and the same types of formation encountered in the previous lines (Fig. 4).

From the topographical point of view, the region of Qsob river presents the subsided zone of this profile going to the South and to the North the altitude of the land becomes important. This line highlights sandstone formations with significant thickness in the North of profile with a resistivity exceeding 250 Ohm.m. They plunge towards the region of Agadir Chicht becomes very reduced in thickness and less resistivity at the level of the region of Qsob river due to the rise of formations of Upper Cretaceous age by the effect of a set of faults of diapiritic origin (Fig. 17).

Going south, the altitude increases and the thickness of resistant R_1 becomes important, it rests directly on a conductive layer C_2 can correspond to plastic marls of Cenomanian age.

7. Conclusion

The geophysical study by vertical electric soundings (VES) and by electric imaging (ERT) carried out within the framework of the recognition of different aquifers in the coastal zone of Essaouira, guided us to very important information on the distribution spatial apparent resistivities and their variations (lateral and vertical). The analysis of the various quantitative and qualitative maps made it possible to follow the roof and the wall of the various aquifers (Plio-Pleistocene and Cretaceous) and aquicludes of the study area.

The results mentioned in the results and discussion section show that the Upper Cretaceous reservoir is by far the most important aquifer in terms of its extension and its hydrodynamic characteristics. It constitutes a multi-layered system and brings together the geological formations, namely the dolomitic limestones and dolomites of the Santonian, the fissured and karstified limestones of the Turonian and the lumachellic limestones and marls of the Cenomanian. The base of this system is formed by the massive dolomitic limestones of the Vraconian. These aquifer properties are linked to the existence of discontinuities within these formations, represented by the stratification planes, sometimes giving rise to water sources, by fracturing and also by the development of karstification phenomena. The Cretaceous aquifer system, is formed by an assemblage of uplifted and subsided blocks separated by faults. These are organized according to three major directions (NNE-SSW, NNW-SSE and EW), which are at the regional scale and correspond to the reactivation of deep faults in the Hercynian basement.

The analysis of the results obtained shows that the area around the Qsob river, is of significant interest from a hydrogeological point of view. It is represented by a very important layer given the wide extension of the resistant formations of Plio-Pleistocene and Cretaceous age with very large thicknesses, it is crossed by the Qsob river which presents as the main source of supply for these two aquifers. The electrical discontinuities emerging from the superposition of the different maps (qualitative and quantitative) and from the tomographic sections are very abundant and dense in the Haha Nord region (Qsob river) with general directions EW, NE-SW and NNE- SW (Piqué and Laville, 1996 ; Piqué et al., 1998 ; Hafid, 2000; Mader et al., 2017 ; Ouzerbane et al., 2021a). They can play a role of drain or main axis of groundwater flow within this aquifer system, as they can constitute impermeable barriers and therefore prevent any flow. Due to this block configuration of the aquifer, the hydrodynamic flow of the aquifer is discontinuous. There may be hydrodynamic interconnections between neighboring blocks thanks in particular to these conductive faults (Ouzerbane et al., 2021a). They also give rise to springs in areas where groundwater drains surface water.

On the other hand, the realization of the tomographic sections from the data of the interpolation by Kriging of the inverted and interpreted vertical electric soundings gave very important information on the structure and the geometry of underground, thereafter they confirm the location of various electrical discontinuities, which may be faults of regional direction already mentioned in the preceding paragraphs.

The lines studied in this study are complementary. An assembly of the eight-resistivity models of these lines provides an overview of the variation in resistivity in the EW and NS direction through the prospected

area. It should be remembered that the location of these lines was guided by existing hydrogeological wells in order to better clarify the structure of the deep basement of the study area.

Given the strong resistivity contrast between the sandstones, limestones, marls and clays, the highlighting of such structures would have been very obvious. The sandstone masses appear clearly on the pseudo-sections and are materialized on the ground by the dominant reliefs, separated from the overlying terrains by regional faults trending NE-SW.

The structure of the region is thus fragmented and fragmented into shreds of anticlines and synclines of reduced dimensions compared to the western part. This discontinuous and folded structure favored the establishment of diapirs of unequal importance. To the north of the lines studied, the fragmented structures gave way to more monotonous stratigraphic forms.

Declarations

Acknowledgements

We are greatly indebted to the Faculty of Science, Moulay Ismail University - Meknes and for granting part of this study. The logistic support during exploration and sampling was funded by the Faculty of Science and Technology, Sultan Moulay Slimane University - Beni Mellal (Morocco). We are also greatful to anonymous reviewers for the fruitful remarks that helped to improve the manuscript.

Competing Interests

The authors have no relevant financial or non-financial interests to disclose.

Author Contributions

All authors have made a significant contribution to this research. Zakaria Ouzerbane, Abdellah El Hmaidi, Ali Essahlaoui and Abdessamad Najine conceived the research idea and designed the framework of the research. Zakaria Ouzerbane and Abdessamad Najine participate in the fieldwork. Zakaria Ouzerbane, Abdellah El Hmaidi and Abdelhadi El Ouali wrote the paper. Zakaria Ouzerbane, Ali Essahlaoui contributed Data processing and model creation. Ouzerbane Zakaria revised the paper.

References

1. Akintorinwa, O.J., Abiola, O., 2011. Subsoil evaluation for pre-foundation study using geophysical and geotechnical approach. Journal of Emerging Trends in Engineering and Applied Sciences, 2(5), 858–863.
2. Alfaifi, H., Kahal, A., Albassam, A., Ibrahim, E., Abdelrahman, K., Zaidi, F., Alhumidan, S., 2019. Integrated geophysical and hydrochemical investigations for seawater intrusion: a case study in southwestern Saudi Arabia. Arabian Journal of Geosciences, 12:372. https://doi.org/10.1007/s12517-019-4540-8

3. Ambroggi, 1963. Etude géologique du versant méridional du Haut Atlas occidental et de la plaine de Souss. Note et mémoire du Service géologie. Maroc, 157, 321pp.
4. Anechana, R., Noye, R.M., Menyeh, A., Manu, E., Okrah, C., 2015. Electromagnetic and vertical electrical sounding for groundwater potential Assessment of Kintampo North Municipality of Ghana. Journal of Environmental Earth Sciences, ISSN 2224–3216 (paper) ISSN 225–0948 5(12).
5. Asfahani, J., 2016. Hydraulic parameters estimation by using an approach based on vertical electrical soundings (VES) in the semi-arid Khanasser valley region, Syria. Journal of African Earth Sciences, 117, 196–206. https://doi.org/10.1016/j.jafre arsci.2016.01.018
6. Attwa, M., Zamzam, S., 2020. An integrated approach of GIS and geoelectrical techniques for wastewater leakage investigations: Active constraint balancing and genetic algorithms application, Journal of Applied Geophysics, 175, 103992. https://doi.org/10.1016/j.jappgeo.2020.103992
7. Atzemoglou, A., Sourlos, P.T., 2012. 2D interpretation of vertical electrical soundings: application to the Sarantaporon basin (Thessaly, Greece). Journal of Geophysics and Engineering, 9, 50–59. doi:10.1088/1742-2132/9/1/006
8. Bahir, M., Jalal, M., Mennani, A., 2001. Pollution nitratée des eaux souterraines du bassin synclinal d'Essaouira. Journal of Environmental Hydrology, 18(9), 1–9.
9. Bahir, M., Ouazar, D., Ouhamdouch, S., 2019. Dam effect on groundwater characteristics from area under semi-arid climate: case of the Zerrar dam within Essaouira basin (Morocco). Carbonates and Evaporites, 34(3), 709–720. https://doi.org/10.1007/s13146-019-00497-0
10. Bose, R.N., Ramkrishna, TS., 1978. Electrical resistivity surveys for ground water in the Deccan trap country of Sangli district, Maharashtra. Journal of Hydrology, 38, 209–221.
11. Basokur, A.T., 1999. Automated 1D interpretation of resistivity soundings by simultaneous use of the direct and iterative methods. Geophysical Prospecting, 47, 149–177.
12. Bersi, M., Saibi, H., 2020. Groundwater potential zones identification using geoelectrical sounding and remote sensing in Wadi Touil plain, Northwestern Algeria. Journal of African Earth Sciences, 172, 104014. https://doi.org/10.1016/j.jafrearsci.2020.104014
13. Bhattacharya, P.K., Patra, H.P., 1968. Direct current geoelectric sounding: principles and interpretation. *Elsevier Science Publishing Co.*, Inc., Amsterdam, 144p.
14. Boswinkel, J.A., 2000. Information Note, International Groundwater Resources Assessment. Centre (IGRAC), Institut néerlandais de géosciences appliquées, Pays-Bas.
15. Broughton, P., Trépanier, P., 1993. Hydrocarbon generation in the Essaouira Basin of western Morocco. A.A.P.G. Bulletin, 77(6), 999–1015.
16. Calow, R.C., Macdonald, A.M., Nicol, A.L., Robins, N.S., 2010. Ground water security and drought in Africa: linking availability, access, and demand. Ground Water, 48, 246–256. https://doi.org/10.1111/j.1745-6584.2009.00558.x
17. Chafouq, D., El Mandour, A., El Gettafi, M., Himi, M., Chouikri, I., Casas, A., 2018. Hydrochemical and isotopic characterization of groundwater in the Ghis-Nekor plain (Northern Morocco). Journal of African Earth Sciences, 139, 1–13. https://doi.org/10.1016/j.jafrearsci.2017.11.007

18. Chamchati, H., Bahir, M., 2013. Potential hydrogeological, environment and vulnerability to pollution of the Plio-Quaternary aquifers of the coastal basin of Essaouira (Morocco). Journal of Environmental Earth Sciences, 3(10), 170–185.
19. Chandra, S., Nagaiah, E., Reddy, D.V., Ananda Rao, V., Ahmed, S., 2012. Exploring deep potential aquifer in water scarce crystalline rocks. J. Earth Syst. Sci., 121(6):1455–1468
20. Choubert, G. & Faure-Muret, A., 1962. Evolution du domaine atlasique marocain depuis les temps paléozoïque. Soc. Géol. France, 1, pp. 447–527.
21. Choubert, G. & Faure-Muret, A., 1956. Lexique stratigraphique du Maroc. Notes Mém. Serv. Géol. Maroc, 134, 165p.
22. Cohen, K.M., Finney, S.C., Gibbard, P.L., Fan, J.-X., 2020. The ICS International Chronostratigraphic Chart. Episodes, 36, 199–204. http://www.stratigraphy.org/ICSchart/ChronostratChart2020-03.pdf
23. Devi, S.P., Srinivasulu, S., Raju, K.K., 2001. Delineation of groundwater potential zones and electrical resistivity studies for groundwater exploration. Environmental Geology, 40,1252–1264.
24. Dey, A., Morrison, H., 1979. Resistivity modelling for arbitrarily shaped two-dimensional structures. Geophysical Prospecting, 27, 106–136. https://doi.org/10.1111/j.1365-2478.1979.tb00961.x
25. Duffaud, F., 1970a. Carte géologique du Maroc au 1/100000, feuille de Tamanar. Note et mémoire du Service géologie. Maroc, 201.
26. Duffaud, F., Brun, & Planchot B., 1966. Bassin du sud-ouest marocain. In: Reyre (ed), Bassin sédimentaire littoral africain. Ass. Serv. Géol. Africain. 1ère partie, Paris, p. 5–12.
27. Ebraheem, A.M., Sherif, M.M., Al Mulla, M.M., Akram, S.F., Shetty, A.V., 2012. A geoelectrical and hydrogeological study for the assessment of groundwater resources in WadiBih, UAE. Environmental Earth Sciences, 67(3),845–857.
28. El Bouhaddioui, M., Mridekh, A., Kili, M., El Mansouri, B., El Gasmi, E., Magrane, B., 2016. Electrical and well log study of the Plio-Quaternary deposits of the southern part of the Rharb Basin, northern Morocco. Journal of African Earth Sciences, 123, 110–122.
29. Eluwole, A.B., Olorunfemi, M.O., Ademilu, O.L., 2018. Soil horizon mapping and textural classification using micro soil electrical resistivity measurements: case study from Ado-Ekiti, southwestern Nigeria. Arabian Journal of Geosciences, 11:315. https://doi.org/10.1007/s12517-018-3652-x
30. Essahlaoui, A., 2000. Contribution à la reconnaissance des formations aquifères dans le bassin de Meknès-Fès (Maroc). Prospection géo-électrique, étude hydrogéologique et inventaire des ressources en eau. *Thèse de Doctorat*, Ecole Mohamadia des Ingénieurs, Rabat, Morocco, 258p.
31. Essahlaoui, A., Sahbi, H., Bahi, L., El Yamine, N., 2001. Preliminary survey of the structure and hydrogeology of the western Saiss Basin, Morocco, using electrical resistivity. Journal of African Earth Sciences, 32(4), 777–789. https://doi.org/10.1016/S0899-5362(02)00054-4
32. Essahlaoui, A., El Ouali, A., 2003. Détermination de la structure géologique de la partie Sud de la plaine du Saïss (bassin de Meknès-Fès, Maroc) par la méthode géoélectrique. Bulletin of Engineering Geology and Environment, 62, 155–166. https://doi.org/10.1007/s10064-002-0178-x

33. Fekri, A., 1993. Contribution à l'étude hydrogéologique et hydrogéochimique de la zone synclinale d'Essaouira (Bassin synclinal d'Essaouira). *Thèse 3ème cycle*, Marrakech, 172p.
34. Flathe, H., 1955. Possibilities and limitations in applying geoelectrical methods to hydrogeological problems in the coastal areas of North West Germany. Geophysical Prospecting, 3, 95–110.
35. Fon, A.N., Che, V.B., Cheo, E.S., 2012. Application of electrical resistivity and chargeability data on a GIS platform in delineating auriferous structures in deeply weathered lateritic terrain, Eastern Cameroun. International Journal of Geosciences, 3, 960–971.
36. Francese, R., Mazzarini, F., Bistacchi, A.L.P., Morelli, G., Pasquare, G., Praticelli, N., Robain, H., Wardell, N., Zaja, A., 2009. A structural and geophysical approach to the study of fractured aquifers in the Scansano-Magliano in Toscanaridge, southern Tuscany, Italy. Hydrogeology Journal, 17,1233–1246
37. Fuh, S.C., Liu, H.C., Ku, C.Y., Chang, T.Y., 2019. 1D Vertical electrical sounding method applied to evaluate shallow gas potential associated with the Hsinying and the Niushan fields in SW Taiwan. *SEG International Exposition and 89th Annual Meeting*, 1179–1183. 10.1190/segam2019-3200645.1
38. Geoscan-M Ltd., 2001. IPI2Win v.2.1, IPI_Res2, IPI_Res3 User's Guide. Moscow State University, 25p.
39. Ghosh, D.P., 1971. The application of linear filter theory on the direct interpretation of geoelectrical resistivity sounding measurements. Geophysical Prospecting, 19, 192–217.
40. Gupta, P.K., Nirwas, S., Gaur, V.K., 1997. Straightforward inversion of vertical electrical sounding data. Geophysics, 62(3), 775–785. https://doi.org/10.1190/1.14441 87
41. Hafid, M., 2000. Triassic-early Liassic extensional systems and Tertiary inversion, Essaouira Basin (Morocco). Marine and Petroleum Geology, 17, 409–429.
42. Himi, M., Tapias, J., Benabdelouahab, S., Salhi, A., Rivero, L., Elgettafi, M., El Mandour, A., Stitou, J., Casas, A., 2017. Geophysical characterization of saltwater intrusion in a coastal aquifer: The case of Martil-Alila plain (North Morocco). Journal of African Earth Sciences, 126, 136–147. https://doi.org/10.1016/j.jafrearsci.2016.11.011
43. Hodlur, G.K, Dhakate, R., Andrade, R., 2006. Correlation of vertical electrical sounding and borehole-log data for delineation of saltwater and freshwater aquifers. Geophysics, 71(1), G11–G20. https://doi.org/10.1190/1.2169847
44. Jamaa, H., El Achheb, A., Ibno Namr, K., 2020. Spatial variation of groundwater quality and assessment of water table fluctuations in Plio-Quaternary aquifer formations in Doukkala Plain, Morocco. Groundwater for Sustainable Development, 11. https://doi.org/10.1016/j.gsd.2020.100398
45. Karroum, M., El Guettafi, M., El Mandour, A., Wilske, C., Himi, M., Casas, A., 2017. Geochemical processes controlling groundwater quality under semi-arid environment: A case study in central Morocco. Science of the Total Environment, 609, 1140–1151. https://dx.doi.org/10.1016/j.scitotenv.2017.07.199
46. Kosinky, W.K., Kelly, W.E., 1981. Geoelectrical sounding for predicting aquifer properties. Groundwater, 19, 163–171.
47. Kumar, D., Rao, V.A., Nagaiah, E., Raju, P.K., Mallesh, D., Ahmeduddin, M., Ahmed, S.,2010. Integrated geophysical study to decipher potential groundwater and zeolite-bearing zones in Deccan Traps.

Current Science, 98(6),803–814.

48. Kumar, D., Rao, V.A., Sarma, V.S., 2014. Hydrogeological and geophysical study for deeper groundwater resource in quarzitic hard rock ridge region from 2D resistivity data. Journal of Earth System Science, 123(3), 531–543.
49. Loke, M.H., 2010. Tutorial: 2-D and 3-D electrical imaging surveys. 154 p.
50. Loke, M.H. & Barker, R.D., 1996. Rapid least-squares inversion of apparent resistivity pseudosections using a quasi-Newton method. Geophysical Prospecting, 44, 131–152.
51. Mashhad, S.R., Ramazi, H., Asgarpour Shahreza, M., 2020. Assessing the effects of 1D assumption violation in vertical electrical sounding (VES) data processing and interpretation. Acta Geophysica. https://doi.org/10.1007/s11600-019-00384-1
52. Mader, N.K., Redfern, J., El Ouataoui, M., 2017. Sedimentology of the Essaouira Basin (Meskala Field) in context of regional sediment distribution patterns during upper Triassic pluvial events. Journal of African Earth Sciences, 130, 293–318.
53. Manu, E., Agyekum, W.A., Duah, A.A., Mainoo, P.A., Okrah, C., Asare, V.S., 2016. Improving Access to Potable Water Supply using Integrated Geophysical Approach in a Rural Setting of Eastern Ghana. Elixir Environ. & Forestry, 95, 40714–40719.
54. Mazac, O., Kelly, W.E., Landa, I., 1985. A hydrophysical model for relation between electrical and hydraulic properties of aquifers. Journal of Hydrology, 79, 1–19.
55. Medina, F., 1994. Evolution structurale de Haut Atlas Occidental et des régions voisines du Trias à l'actuel, dans le cadre de l'ouverture de l'Atlas Atlantique Centrale et de la collision Afrique-Europe. *Thèse de Doctorat ès-Sciences*, Université Mohammed V, Rabat, Morocco, 272p.
56. Mennani, A., 2001. Apport de l'Hydrochimie et de l'Isotopie à la connaissance du fonctionnement des aquifères de la zone côtière d'Essaouira (Maroc occidental). *Thèse de Doctorat ès-Sciences*, Université Cadi Ayyad, Marrakech, Morocco, 172p.
57. Ogungbe, A.S., Onori, E.O., Olaoye, M.A., 2012. Application of electrical resistivity techniques in the investigation of groundwater contamination. A case study of ille-Epo Dumpsite, Lagos, Nigeria. International Journal of Geomatics and Geosciences, 3(1), 30–41.
58. Okrah, C., Danuor, S.K., Dapaah-Siakwan, S., 2012. Groundwater exploration in granitic rock formation of Komenda/Edina/Eguafo/Abirem district using integrated geophysical techniques. Journal of the Ghana Science Association, 14(2), 56–72.
59. Ouarani, M., Bahir, M., Mulla, DJ., Ouazar, D., Chehbouni, A., Dhiba, D., Ouhamdouch, S., El Mountassir, O., 2020. Groundwater quality characterization in an overallocated semi-arid coastal area using an integrated approach: case of the Essaouira Basin, Morocco. Water 12: 3202. https://doi.org/10.3390/w12113202
60. Ouarani, M., Bahir, M., Mulla, DJ., Ouazar, D., Chehbouni, A., Dhiba, D., 2021. Groundwater quality deterioration and recharge modes in a semi-arid coastal aquifer: Essaouira Aquifer case study (Morocco). Arabian Journal of Geosciences 14:1989, 2–15. https://doi.org/10.1007/s12517-021-08267-w

61. Ouhamdouch, S., Bahir, M., Chkir, N., Carreira, P., Goumih, A., 2016a. Comportement hydrogéochimique d'un aquifère côtier des zones semi-arides: cas de l'aquifère Barrémien-aptien du bassin d'Essaouira (Maroc occidental). Larhyss J 25:163–182
62. Ouhamdouch, S., Bahir, M., Souhel, A., Carreira, PM., 2016b.Vulnerability and impact of climate change processes on water resource in semi-arid areas: in Essaouira basin (Morocco). In: Grammelis P (ed) Energy, transportation and global warming, green energy and technology. Springer International, Cham, pp 719–736. https://doi.org/10.1007/978-3-319-30127-3_53
63. Ouhamdouch, S., Bahir, M., Carreira, PM., 2018a. Impact du changement climatique sur la ressource en eau en milieu semi-aride: exemple du bassin d'Essaouira (Maroc). RSE 31:13–27
64. Ouhamdouch, S., Bahir, M., Ait-Tahar, M., Goumih, A., Rouissa, A., 2018b. Physico-chemical quality and origin of groundwater of an aquifer under semi-arid climate. Case of the Barremo-Aptian aquifer of Essaouira basin (Morocco Occidental). J Mater Environ Sci 9:1022–1034
65. Ouhamdouch, S., Bahir, M., Ouazar, D., Carreira, PM., Zouari, K., 2019. Evaluation of climate change impact on groundwater from semi-arid environment (Essaouira Basin, Morocco) using integrated approaches. Environ Earth Sci 78:449. https://doi.org/10.1007/s12665-019-8470-2
66. Ouzerbane, Z., Najine, A., Aïfa, T., El Hmaidi, A., Essahlaoui, A., Radouani, F., 2013. Etude géophysique par imagerie électrique du système aquifère au Nord-Est du bassin d'Essaouira, Maroc. Journal of Hydrocarbons, Mines and Environmental Research, 4(1), 57–70.
67. Ouzerbane, Z., Najine, A., Aïfa, T., El Hmaidi, A., Essahlaoui, A., 2014. Apport de l'hydrogéophysique et le SIG à l'étude des ressources en eaux dans la partie nord côtière du bassin d'Essaouira-Maroc. Colloque international des Utilisateurs de SIG, TAZA GIS-Days, Morocco. Infrastructure des données spatiales et Application des SIG, 300–306. ISBN: 978-3-8381-4837-3.
68. Ouzerbane, Z., 2015. Contribution de la géophysique, des SIG et de l'analyse multicritère à la reconnaissance des ressources en eau et leur vulnérabilité à la pollution. Cas du sous-bassin côtier d'Essaouira (Maroc). Thèse de Doctorat, Université Moulay Ismail, Meknès, Morocco, 304.
69. Ouzerbane, Z., Boughalem, M., El Hmaidi, A., Essahlaoui, A., Najine, A., Aïfa, T., Redouani, F., El Ouali, A., 2018a. Evaluation des facteurs physiographiques et leurs impacts sur les ressources en eau dans les bassins versants d'Essaouira (Essaouira, Maroc). Journal International Sciences et Technique de l'Eau et de l'Environnement, 3(1), 29–37. ISNN (electronic): 1737–9350; ISSN (printed): 1737–6688.
70. Ouzerbane, Z., El Hmaidi, A., Essahlaoui, A., Najine, A., Aïfa, T., Abbassi, M., El Ouali, A., 2018b. Application de la méthode DRASTIC à l'étude de la vulnérabilité à la pollution des aquifères dans la zone côtière d'Essaouira (Essaouira, Morocco). 4ème édition du Colloque internationale des Utilisateurs des SIG (Meknès GISDAYS2018). Université Moulay Ismail, Faculté des Sciences, p 141, Meknès, les 20–21 décembre 2018.
71. Ouzerbane, Z., Boughalem, M., El Hmaidi, A., Aïfa, T., Essahlaoui, A., El Ouali, A., Najine, A., Redouani, F., Wafik, A., 2019. Application of GIS to study the physiographic factors and the water resources in the watersheds of Essaouira, Morocco. Journal of Water Sciences & Environment Technologies, 4(1), 480–490, ISSN: 2508–9250.

72. Ouzerbane, Z., Aïfa, T., El Hmaidi, A., Essahlaoui, A., Najine, A., 2021a. A geoelectric study of aquifers in the Essaouira coastal region, Morocco. Journal of African Earth Sciences, Volume 183, 2021, 104309, ISSN 1464-343X, https://doi.org/10.1016/j.jafrearsci.2021.104309
73. Ouzerbane, Z., Loulida, S., El Hmaidi, A., Essahlaoui, A., Boughalem, M., Ousmana, H., Berrada, M., 2021b. Study of the salinity of groundwater in the HAHA syncline by the Kohonen self-organized classification (Essaouira, Morocco). Environ Sci Pollut Res. https://doi.org/10.1007/s11356-021-16598-0
74. Ouzerbane, Z., Loulida, S., Boughalem, M., El Hmaidi, A., Essahlaoui, A., Najine, A., 2021c. Application of GIS for assessing the vulnerability of aquifers to pollution in the coastal zone of Essaouira, Morocco. Environ Monit Assess 194:35. https://doi.org/10.1007/s10661-021-09673-z
75. Owen, R.J., Gwavava, O., Gwaze, P., 2005. Multi-electrode resistivity survey for groundwater exploration in the Harare greenstone belt, Zimbabwe. Hydrogeology Journal, 14, 244–252. https://doi.org/10.1007/s10040-004-0420-7
76. Perrone, A., Iannuzzi, A., Lapenna, V., Lorenzo, P., Piscitelli, S., Rizzo, E., Sdao, F., 2004. High resolution electrical imaging of the Varco d'Izzo earthflow (Southern Italy). Journal of Applied Geophysics, 56, 17–29.
77. PNUE, 2008. Vital Water Graphics - An Overview of the State of the World's Fresh and Marine Waters, 2nd Ed, PNUE, Nairobi, Kenya. .
78. Piatti, C., Boiero, D., Godio, A., Socco, L.V., 2010. Improved Monte Carlo 1D inversion of vertical electrical sounding and time-domain electromagnetic data. Near Surface Geophysics, 8, 117–133.
79. Piqué, A., 1994. Géologie du Maroc. Les domaines régionaux et leur évolution structurale. *Presses Universitaires Maghrébins Edition*, Marrakech, Morocco, 284p.
80. Piqué, A., Laville, E., 1996. The central Atlantic rifting: reactivation of Palaeozoic structures? Journal of Geodynamics, 21, 235–255.
81. Piqué, A., Le Roy, P., Amrhar, M., 1998. Transtensive synsedimentary tectonics associated with ocean opening: the Essaouira-Agadir segment of the Moroccan Atlantic margin. Journal of the Geological Society, London, 155, 913–928.
82. Radouani, F., Najine, A., Aïfa, T., Ouzerbane, Z., 2013. Reconnaissance du système aquifère du nord-ouest de la plaine du Tadla (Maroc central) par imagerie électrique. Journal of Hydrocarbons, Mines and Environmental Research, 4(1), 33–41.
83. Rey, J., Canerot, J., Peybernes, B., Taj-Eddine, K., Rahhali, I. & Roch, E., 1950. Histoire stratigraphique du Maroc. Note et mémoire. Ser. Géo. du Maroc, Rabat, N°80, 440p.
84. Reynolds, J. M., 1997. An introduction to applied and environmental geophysics. Chichester: Wiley.
85. Roch, E., 1931. Carte géologique provisoire des Abda, des Jbilets occidentales, de la zone synclinale de Mogador et de l'Atlas occidental.
86. Russell, E.J.F. & Barker, R.D., 2010. Electrical properties of clay in relation to moisture loss. Near Surface Geophysics, vol.8, pp 173–180. DOI: 10, 3997/1873 – 0604, 2010001

87. Sainato, C., Galindo, G., Pomposiello, C., Malleville, H., de Abelleyra, D., Lossino, B., 2003. Electrical conductivity and depth of groundwater at the Pergamino zone (Buenos Aires Province, Argentina) through vertical electrical sounding and geostatistical analysis. Journal of South American Earth Sciences, 161, 177–186. https://dx.doi.org/10.1016/S0895-9811(03)00027-0
88. Sajinkumar, K.S., Castedo, R., Sundarajan, P., Rani, V.R., 2015. Study of a partially failed landslide and delineation of piping phenomena by vertical electrical sounding (VES) in the Wayanad Plateau, Kerala, India. Natural Hazards, 75, 755–778. https://doi.org/10.1007/s1106 9-014-1342-x
89. Shah, T., et al., 2007. Groundwater: A Global Assessment of Scale and Significance », D. Molden (dir. pub.), Water for Food, Water for Life: A Comprehensive Assessment of Water Management in Agriculture, IWMI (Institut international de gestion des ressources en eau), Earthscan Publications, Londres.
90. Sharma, P.V., 1997. Environmental and engineering geophysics. *Cambridge University Press*, 475p.
91. Sharma, S.P., Baranwal, V.C., 2005. Delineation of groundwater-bearing fracture zones in a hard rock area integrating very low frequency electromagnetic and resistivity data. Journal of Applied Geophysics, 57, 155–166. https://doi.org/10.1016/j.jappgeo.2004.10.003
92. Sherif, M., El Mahmoudi, A., Garamoon, H., Shetty, A., 2006. Geoelectrical and hyrogeochemical studies for delineating seawater intrusion in the outlet of Wad, Ham, UAE. Environmental Geology, 49, 536–551
93. Shiklomanov, I. A. and Rodda, J. C., 2003. World Water Resources at the Beginning of the 21st Century, Cambridge University Press, Cambridge, Royaume-Uni.
94. Sikah, J.N., Aning, A.A., Danuor, S.K., Manu, E., Okrah, C., 2016. Groundwater Exploration using 1D and 2D Electrical Resistivity Methods. Journal of Environmental Earth Science, 6(7), 55–63.
95. Sinan, M., Boussetta, M., El Rherari, A., 2009. Changements climatiques: Causes et conséquences sur le climat et les ressources en eau. Séminaire international sur : Le dessalement des eaux. *Recueil des communications, Amicale des Ingénieurs du Génie Rural du Maroc*, Tanger, Morocco, 12–22.
96. Singh, U.K., Tiwari, R.K., Singh, S.B., 2005. One-dimensional inversion of geo-electrical resistivity sounding data using artificial neural networks—a case study. Computers and Geosciences, 31, 99–108. https://doi.org/10.1016/j.cageo.2004.09.014
97. Singh, U.K., Tiwari, R.K., Singh, S.B., 2013. Neural network modeling and prediction of resistivity structures using VES Schlumberger data over a geothermal area. Computers and Geosciences, 52, 246–257. https://dx.doi.org/10.1016/j.cageo.2012.09.018
98. Souid, A., 1983. Etude tectonique et microtectonique des injections du Trias dans le bassin d'Essaouira pendant les compressions alpines dans l'avant-pays atlasique (Maroc). *Thèse de Doctorat 3ème cycle*, Université de Montpellier, France, 101p.
99. Srinivas, Y., Raj, A.S., Oliver, H.D., Muthuraj, D., Chandrasekar, N., 2012. A robust behavior of Feed Forward Back propagation algorithm of Artificial Neural Networks in the application of vertical electrical sounding data inversion. Geoscience Frontiers, 3(5), 729–736. https://dx.doi.org/10.1016/j.gsf.2012.02.003

100. Store, H., Storz, W., Jacobs, F., 2000. Electrical resistivity tomography to investigate geological structures of Earth's upper crust. Geophysical Prospecting, 48,455–471.
101. Taj-Eddine, K., 1991. Le Jurassique terminal et le Crétacé basal dans l'Atlas Atlantique (Maroc), Biostratigraphie, Sédimentologie, Stratigraphie séquentielle et Géodynamique. *Thèse de Doctorat ès-Sciences*, Université Cady Ayyad, Marrakech, Morocco, 285p.
102. Urish, D.W., Frohlich, R.K., 1990. Surface electrical resistivity in coastal groundwater exploration. Geoexploration, 26, 267–289.
103. Wafiq, A., Ec-Chouafi, E., Didi, S., Ouzerbane, Z., Abbari, M., 2019. Hydro-electric study of Bajocian aquifer of Mellaha village, Oued Guir, Errachidia, Morocco. Journal of Water Sciences & Environment Technologies, 4(1), 428–442. ISSN: 2508–9250.
104. Yadav, G.S., Singh, S.K., Srivastava, K.M., 1997. Fast method of resistivity sounding for shallow groundwater Investigations. Journal of Applied Geophysics, 36, 45–52.
105. Yadav, G.S., Abolfazli, H., 1998. Geoelectrical soundings and their relationships to Hydraulic parameters in semiarid regions of Jalore, North West India. Journal of Applied Geophysics, 39, 35–51.
106. Yadav, G.S., Singh, S.K., 2007. Integrated resistivity surveys for delineation of fractures for ground water exploration in hard rock area. Journal of Applied Geophysics, 62(3), 301–312.
107. Zaidi, F.K., Kassem, O.M.K., 2012. Use of electrical resistivity tomography in delineating zones of groundwater potential in arid regions; a case study from Diriyah region of Saudi Arabia. Arabian Journal of Geosciences, 5, 327–333.
108. Zektser, I. S., and Everett, L. G., 2004. Groundwater Resources of the World and Their Use, UNESCO IHP-VI Series on Groundwater, n° 6, UNESCO (Organisation des Nations Unies pour l'éducation, la science et la culture), Paris. http://unesdoc.unesco.org/images/0013/001344/134433e.pdf
109. Zhody, A., 1989. A new method for the interpretation of Schlumberger and Wenner sounding curves. Geophysics, 54(2), 245–253.

Figures

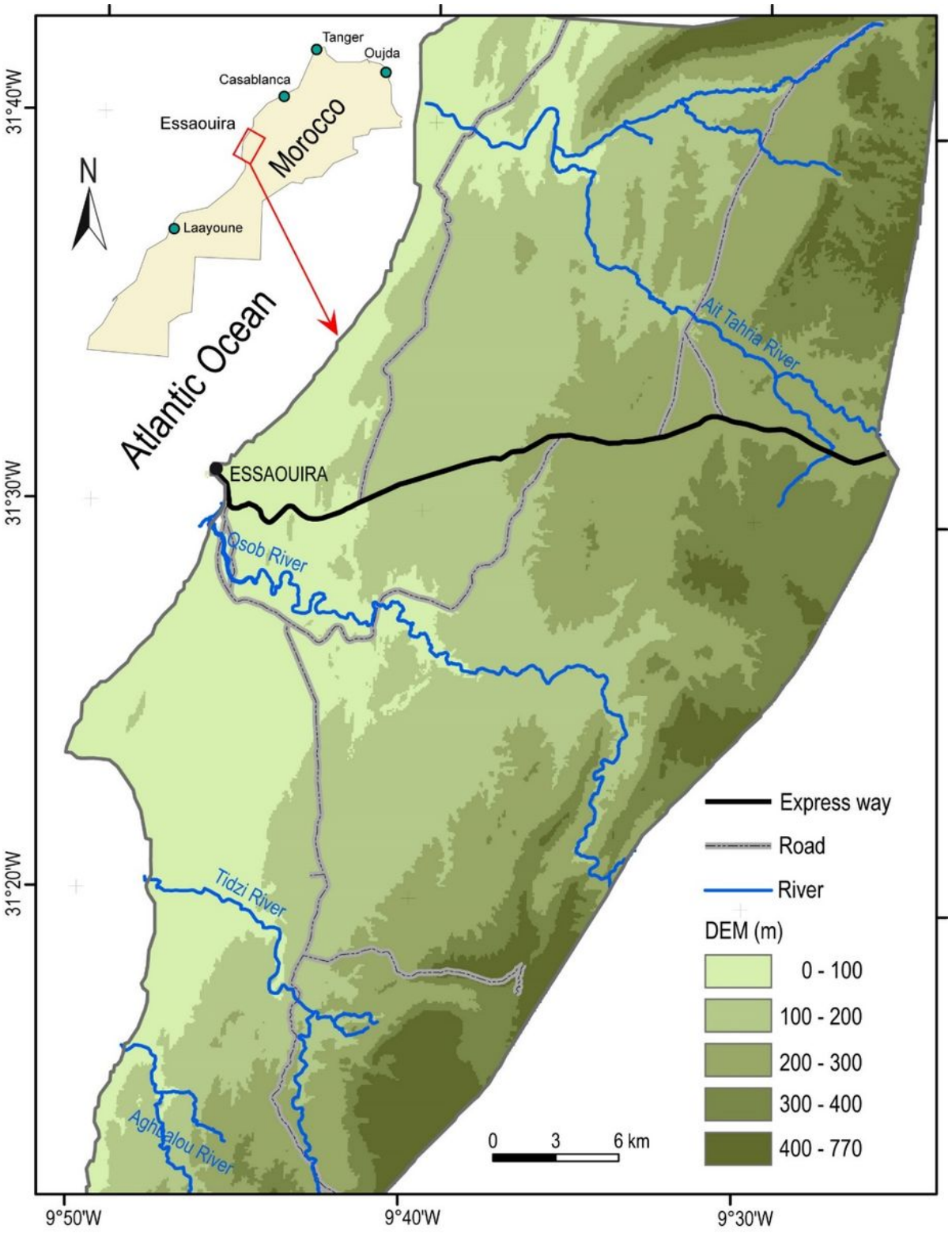

Figure 1

Location of the study area in the coastal of Essaouira (Ouzerbane et al., 2021a)

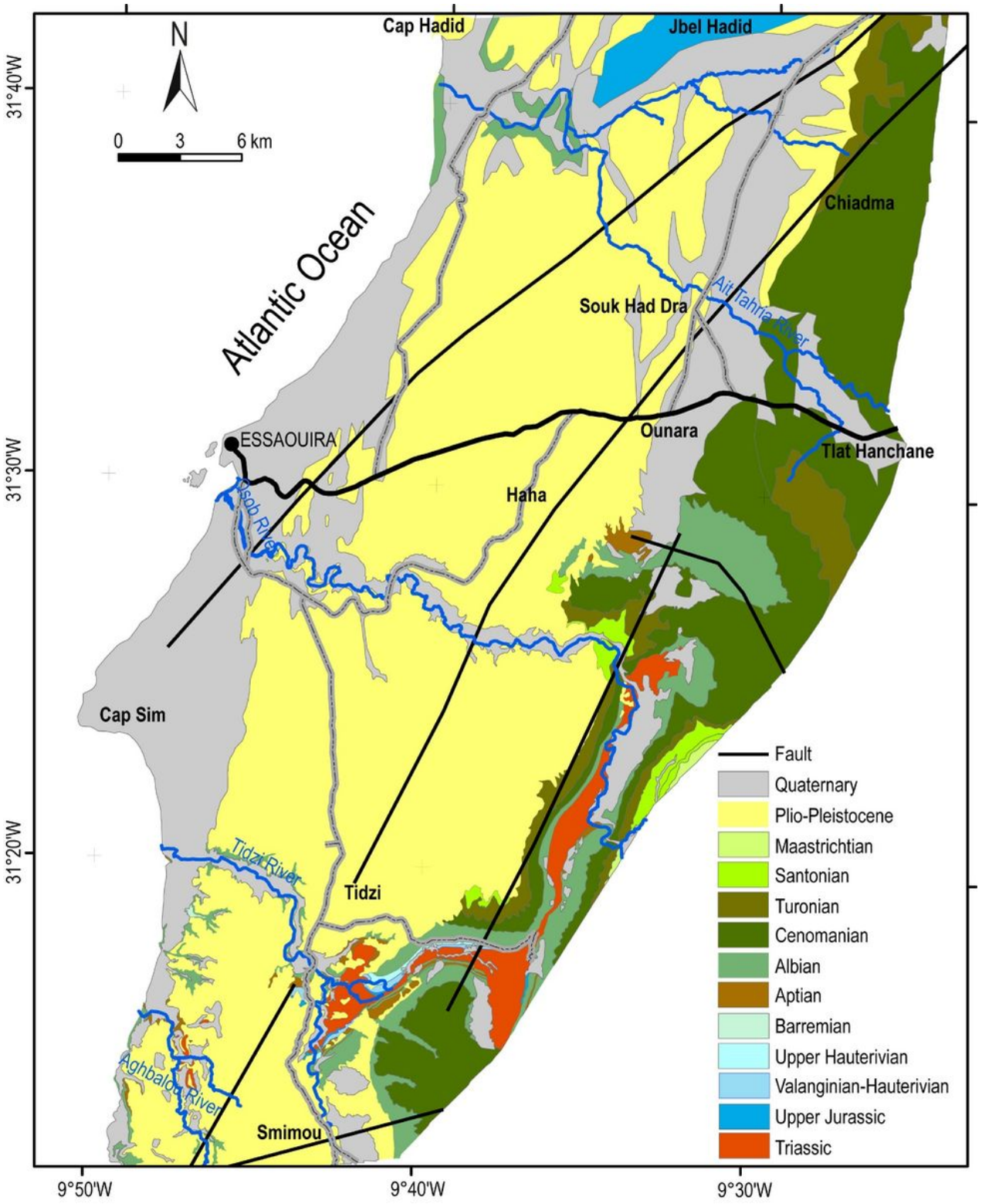

Figure 2

Geological map of the Essaouira coastal zone (Ouzerbane, 2015; Ouzerbane et al., 2019).

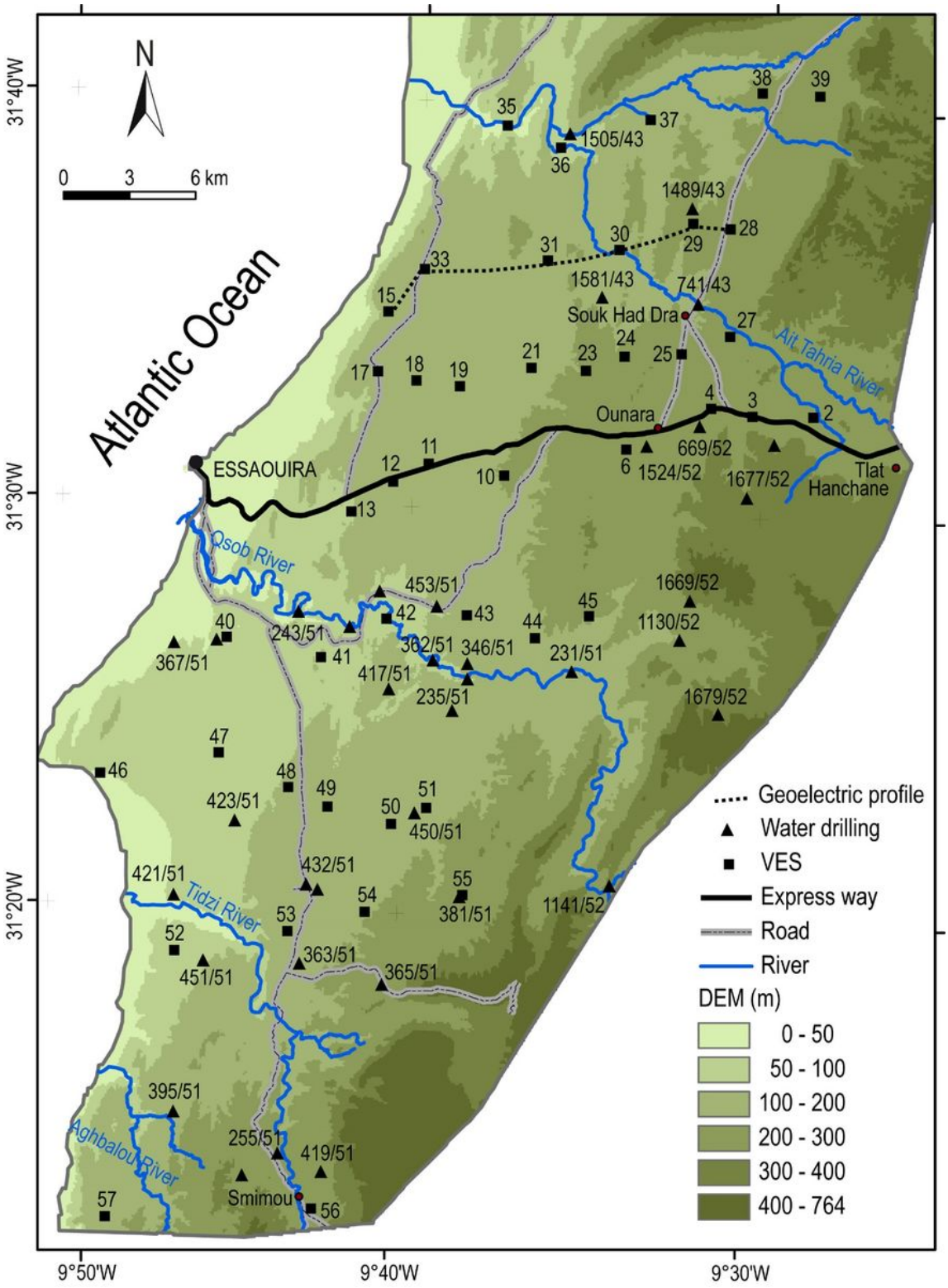

Figure 3

Location of vertical electrical soundings (VES) and the mechanical drillings (MD) in the study area (Ouzerbane et al., 2021a).

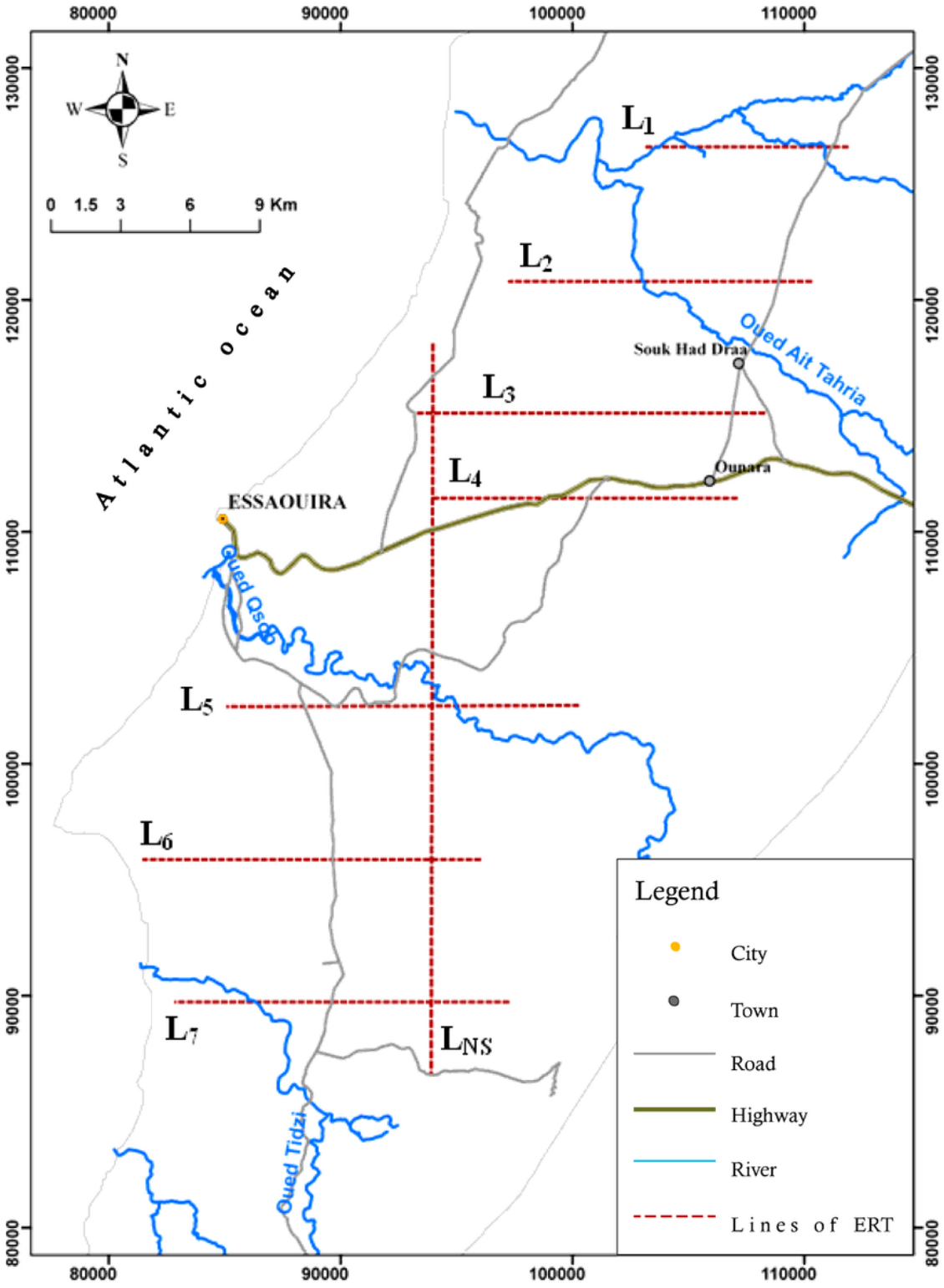

Figure 4

Location of selected lines of electrical resistivity tomography (ERT).

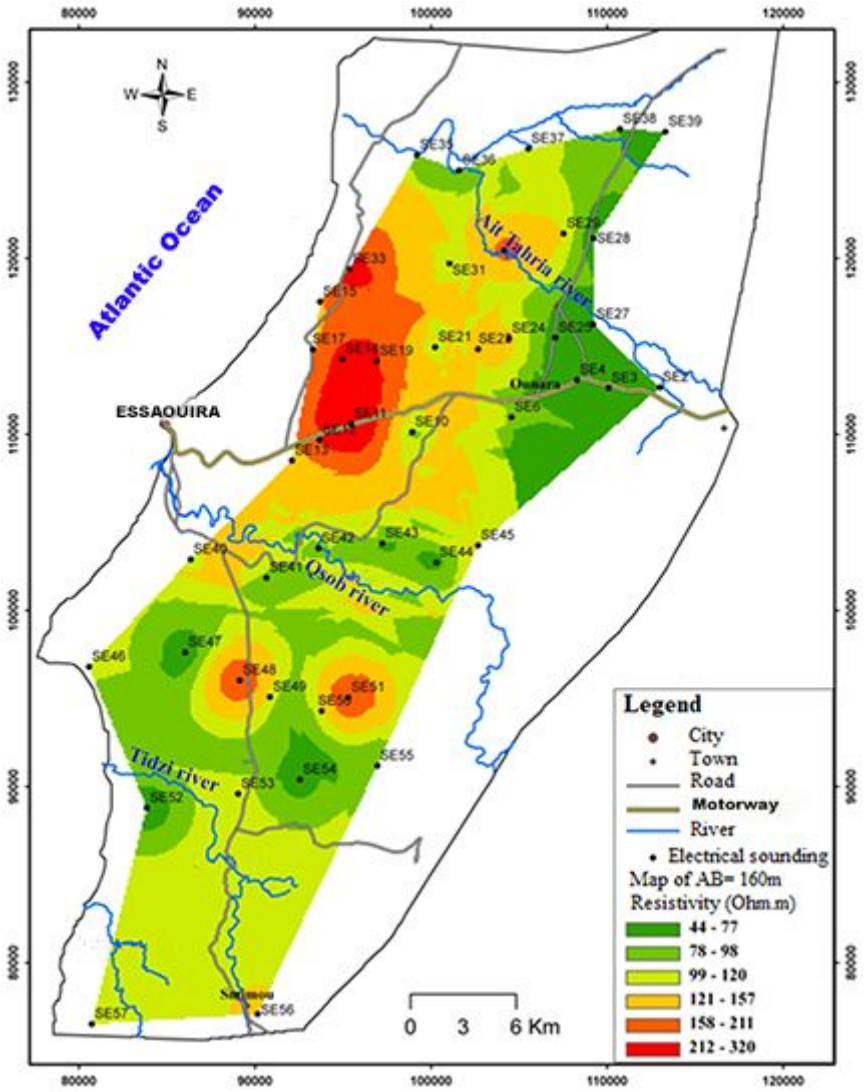

Figure 5

Apparent resistivity map for AB=160 m (Ouzerbane et al., 2021a).

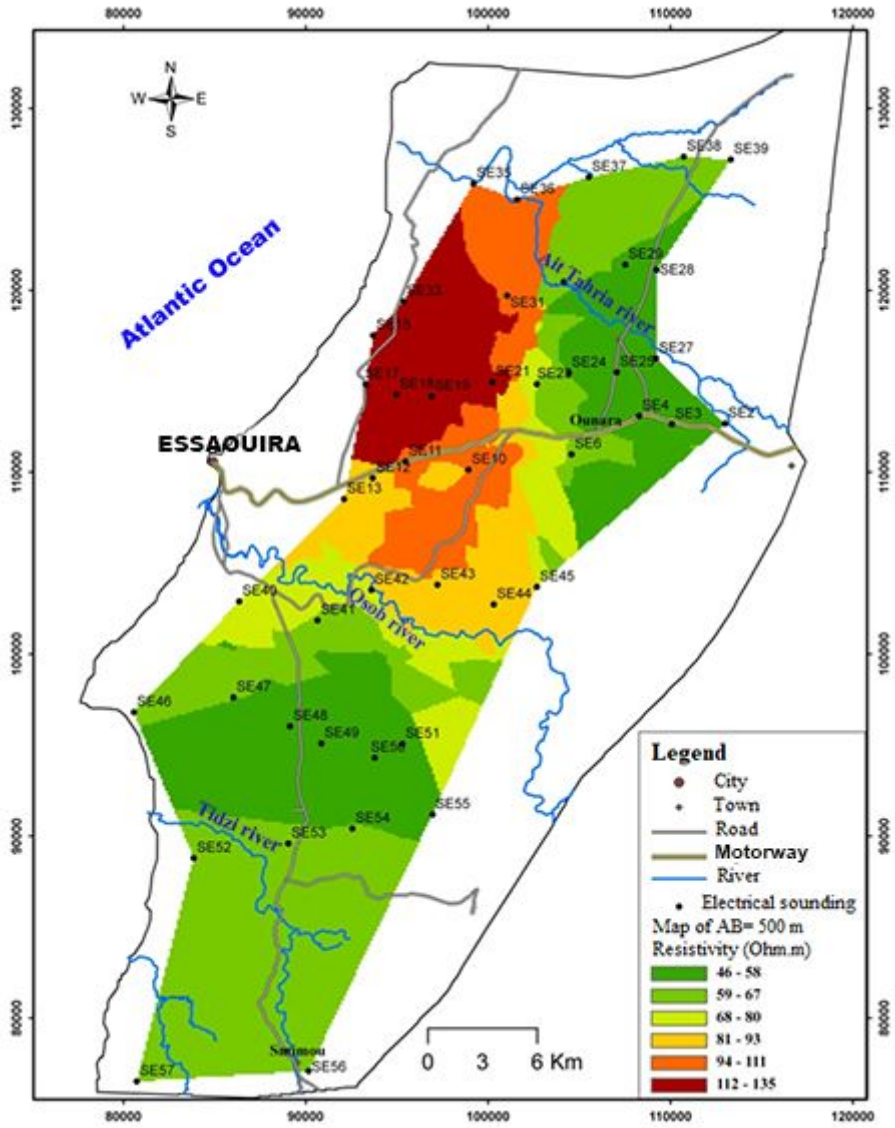

Figure 6

Apparent resistivity map for AB=500 m (Ouzerbane et al., 2021a).

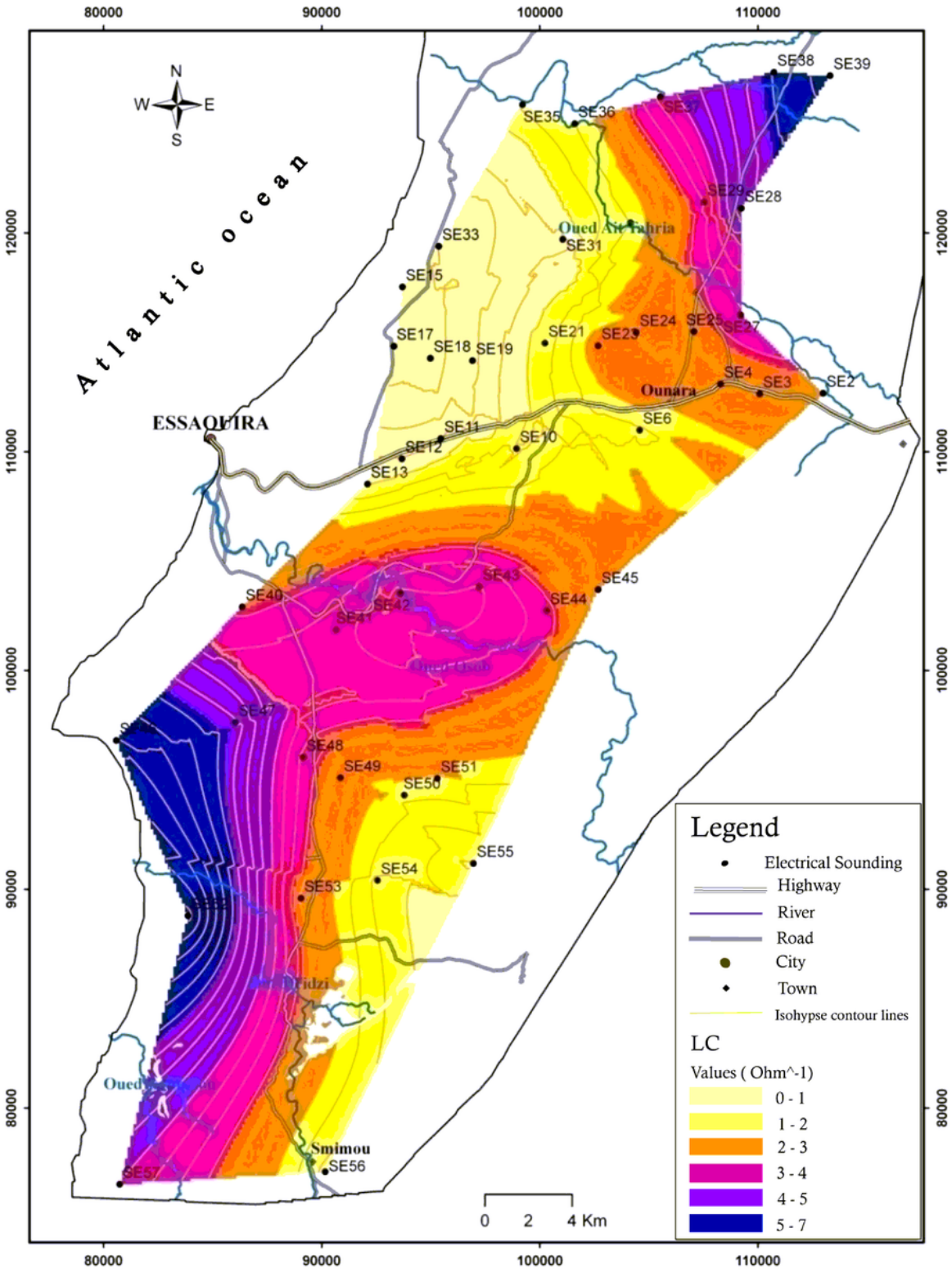

Figure 7

Map of the longitudinal conductance (LC) of the Cretaceous age conductor.

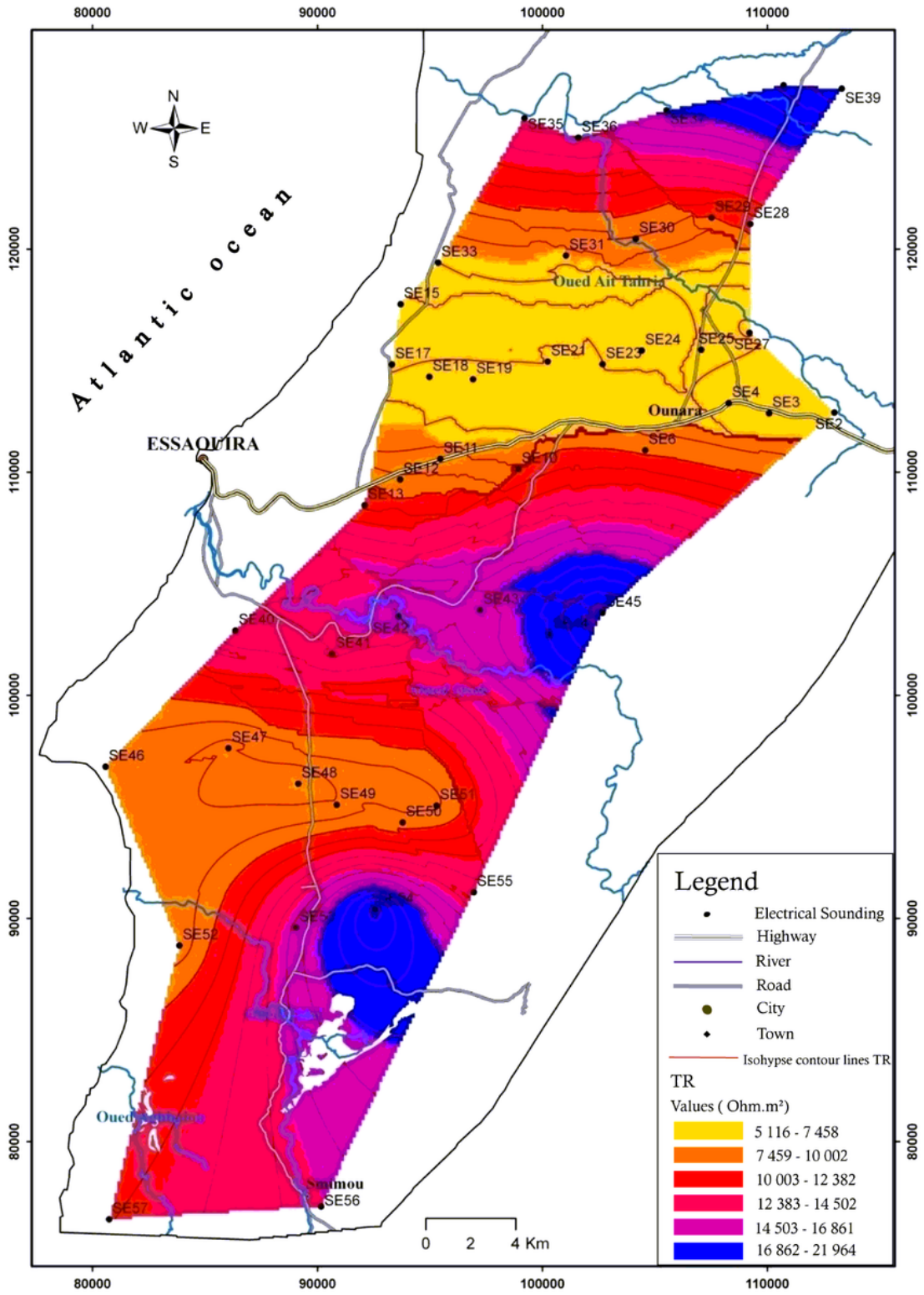

Figure 8

Map of the transverse resistance of the Cretaceous age resistant.

Figure 9

Isohypses Map of the Cretaceous age resistant.

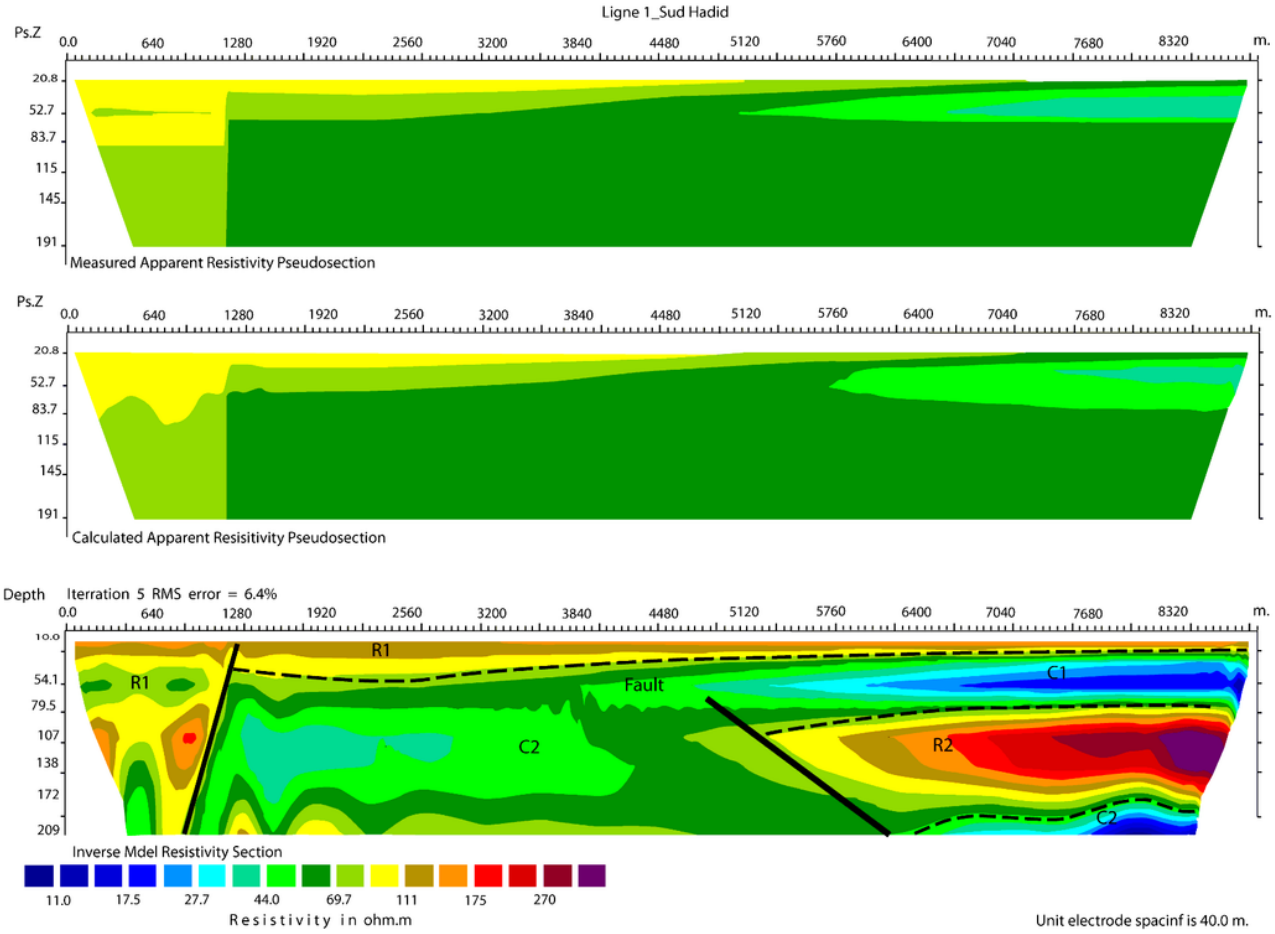

Figure 10

2D electrical imaging section of tomographic line 1 (South Hadid region).

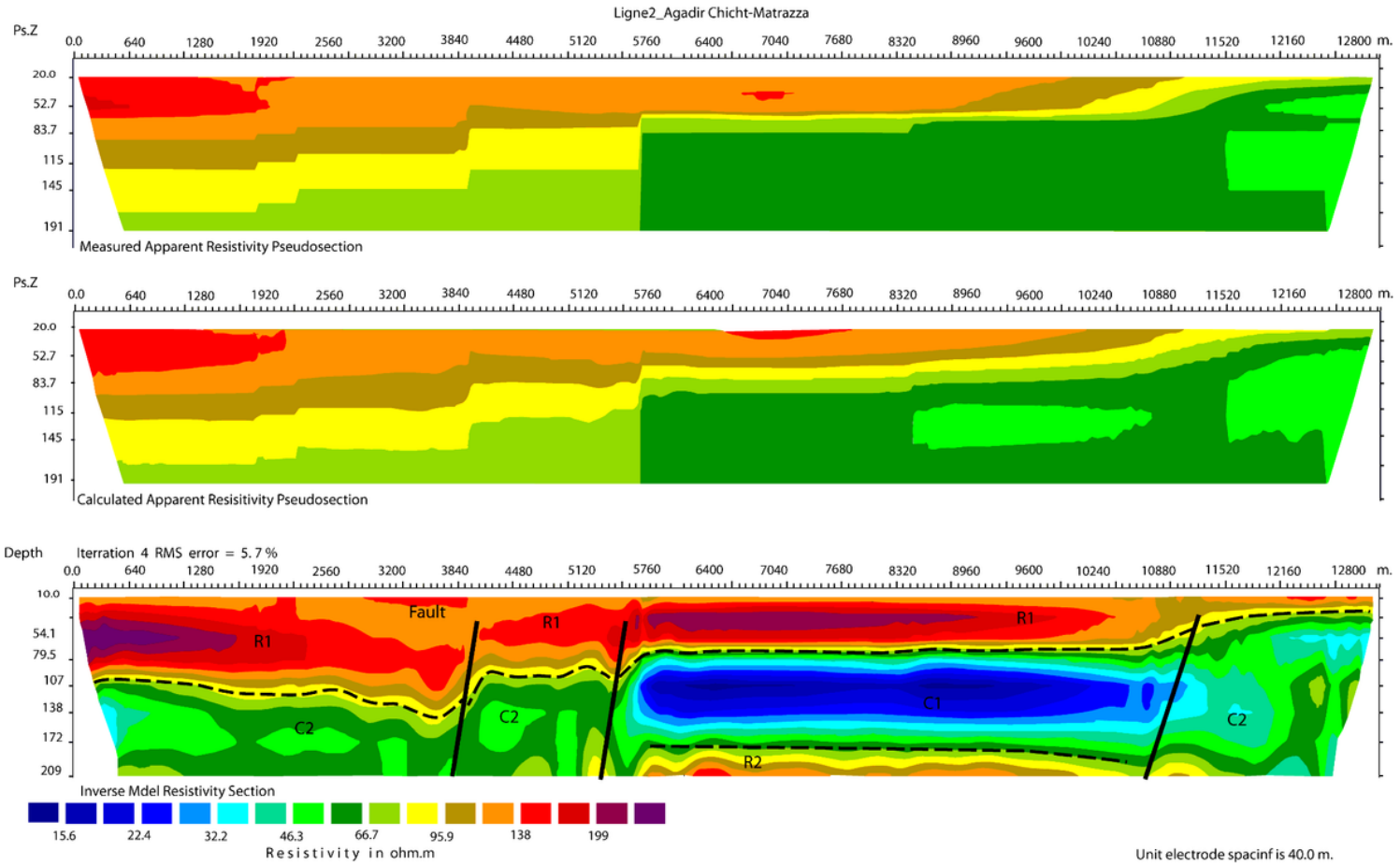

Figure 11

2D electrical imaging section of tomographic line 2 (Agadir Chicht - Matrazza).

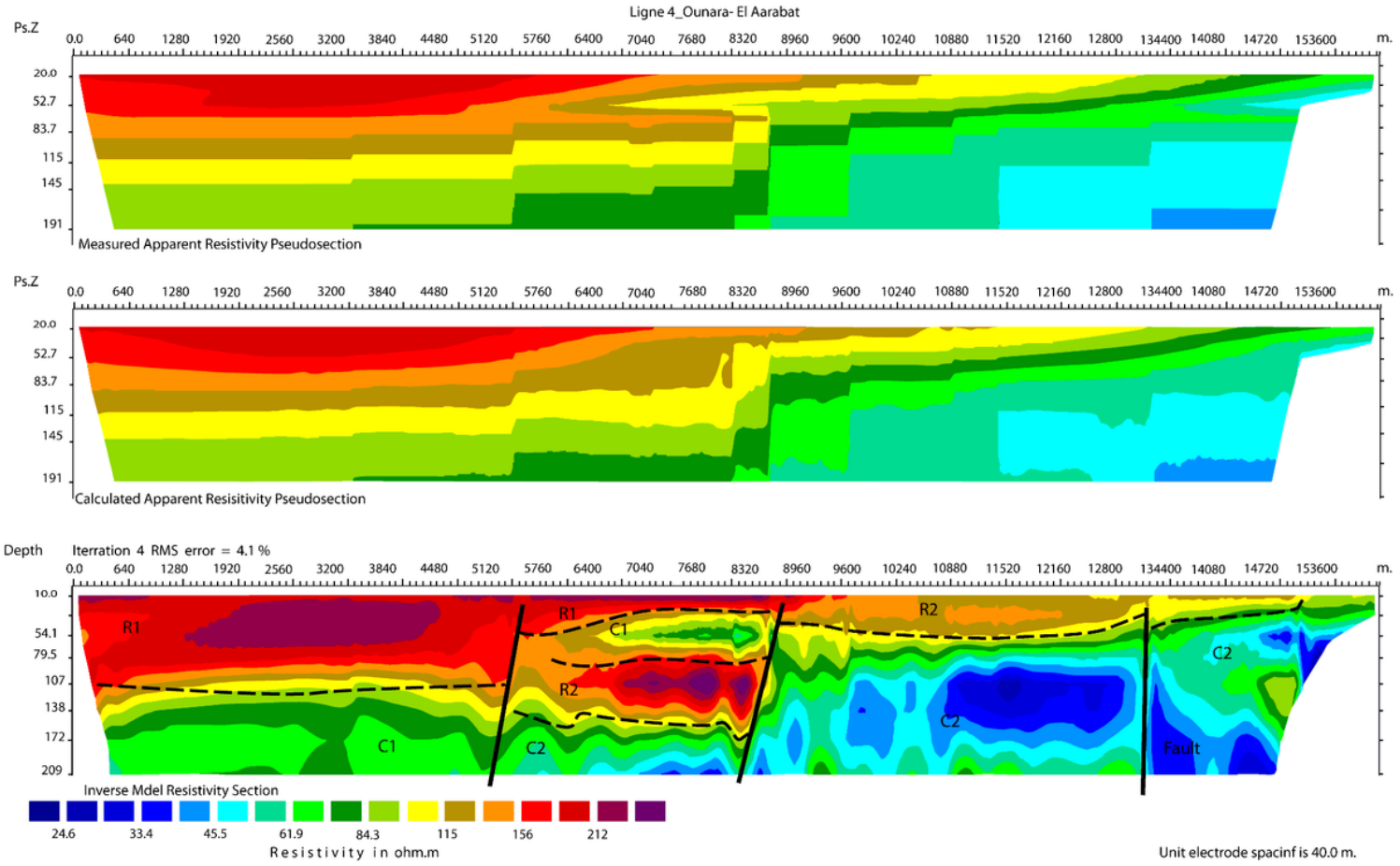

Figure 12

2D electrical imaging section of tomographic line 3 (Agadir Chicht - Matrazza region).

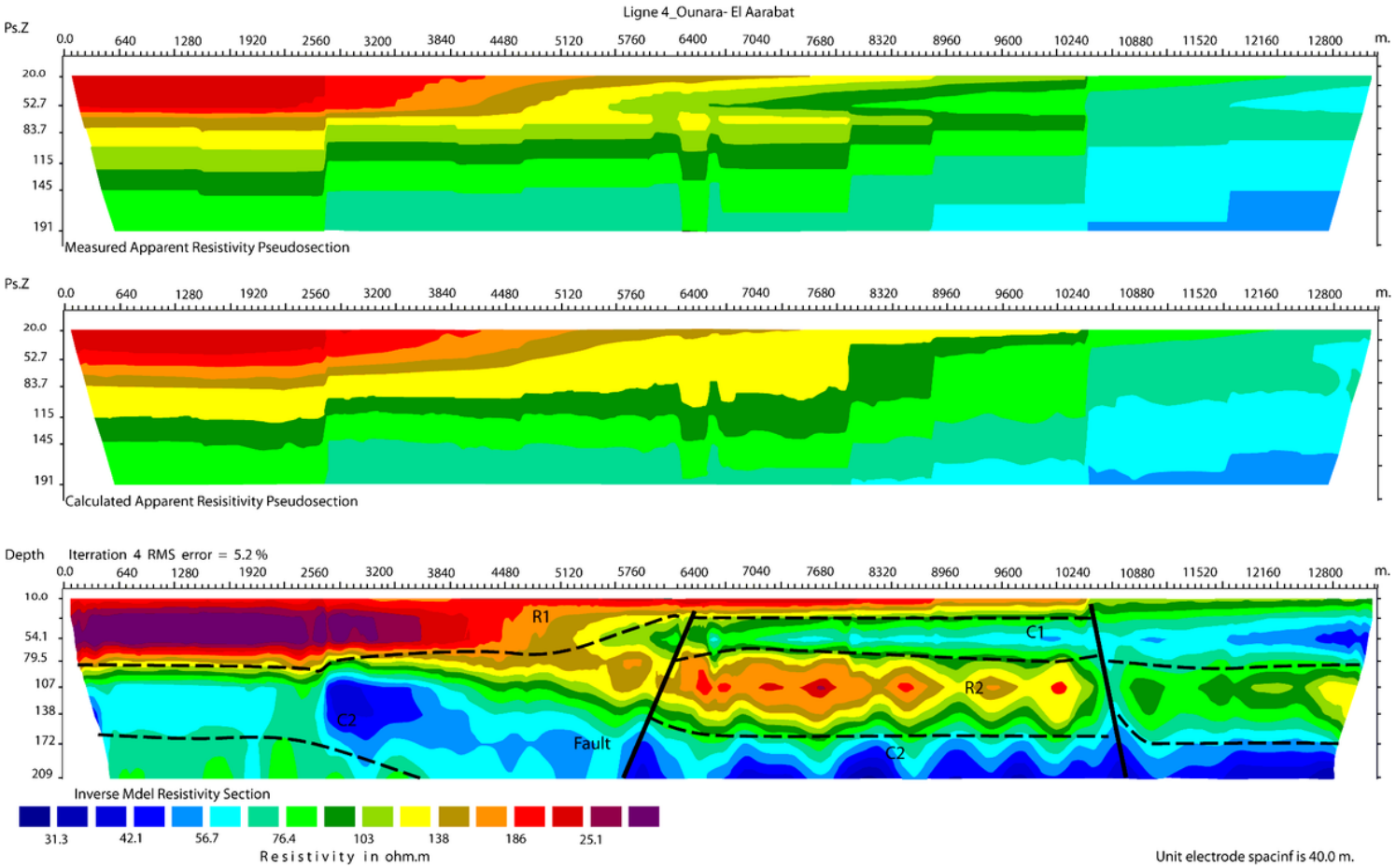

Figure 13

2D electrical imaging section of tomographic line 4 (El Aarabat-Ounara region).

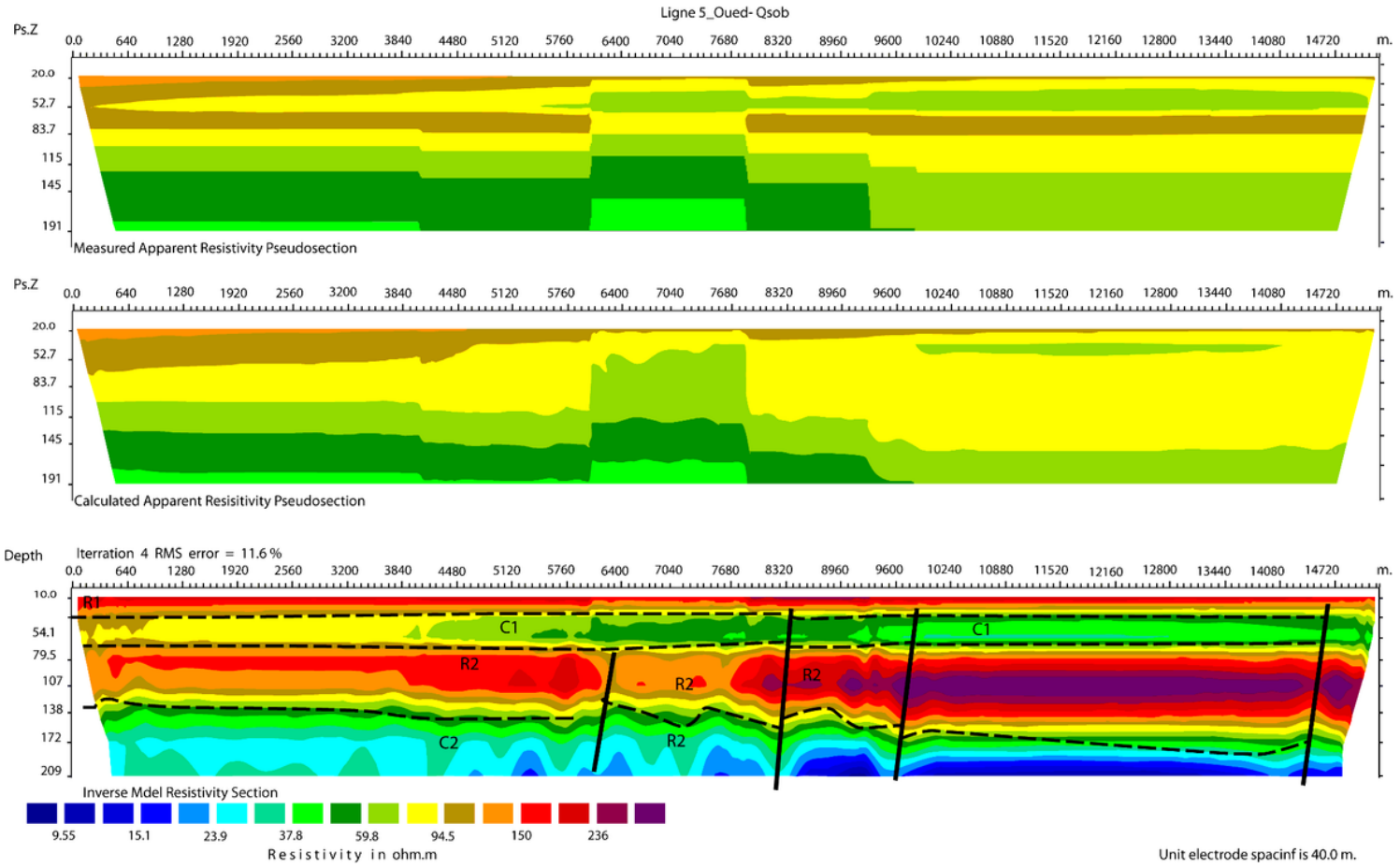

Figure 14

2D electrical imaging section of tomographic line 5 (Qsob river region).

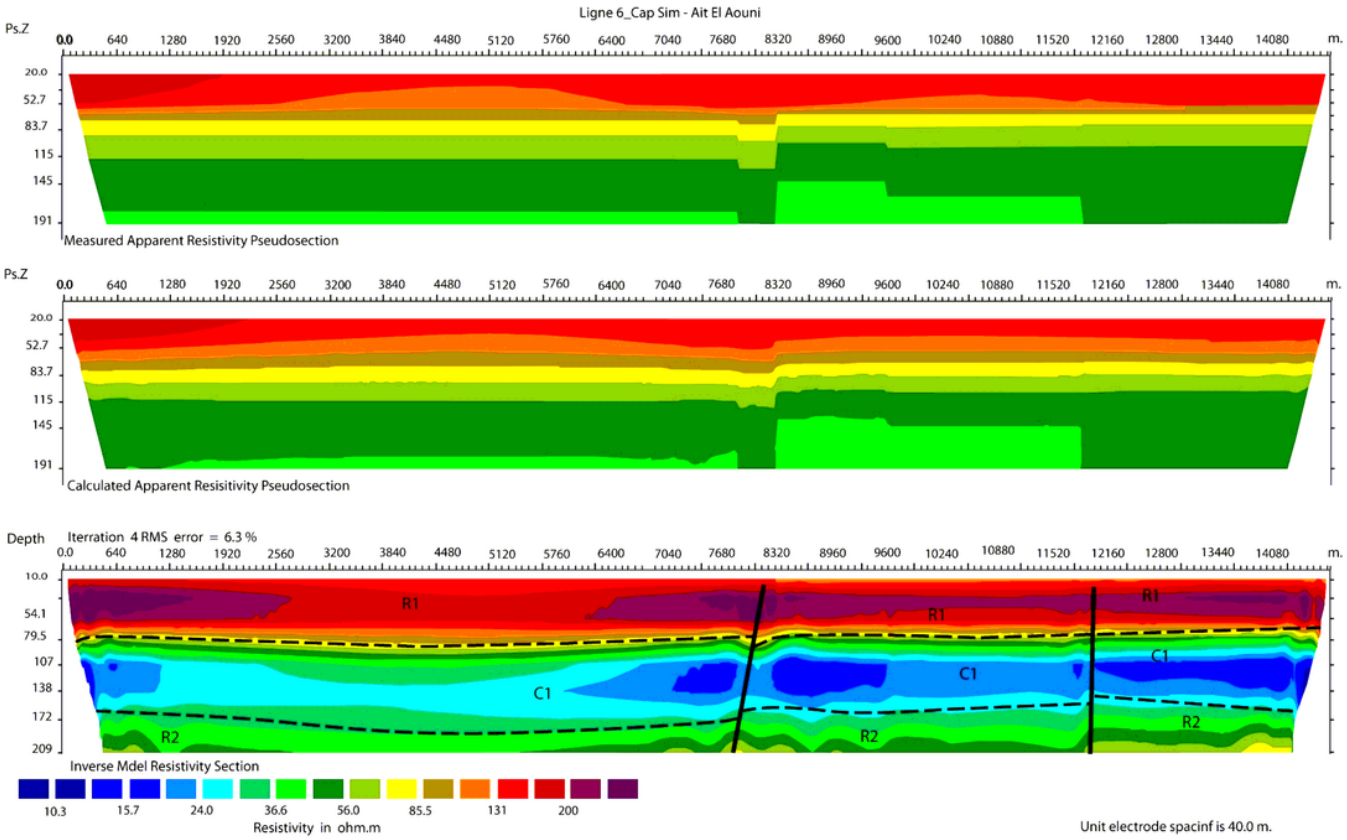

R2 R2 R2

Figure 15

2D electrical imaging section of tomographic line 6 (Cap Sim – Ait El Aouni region).

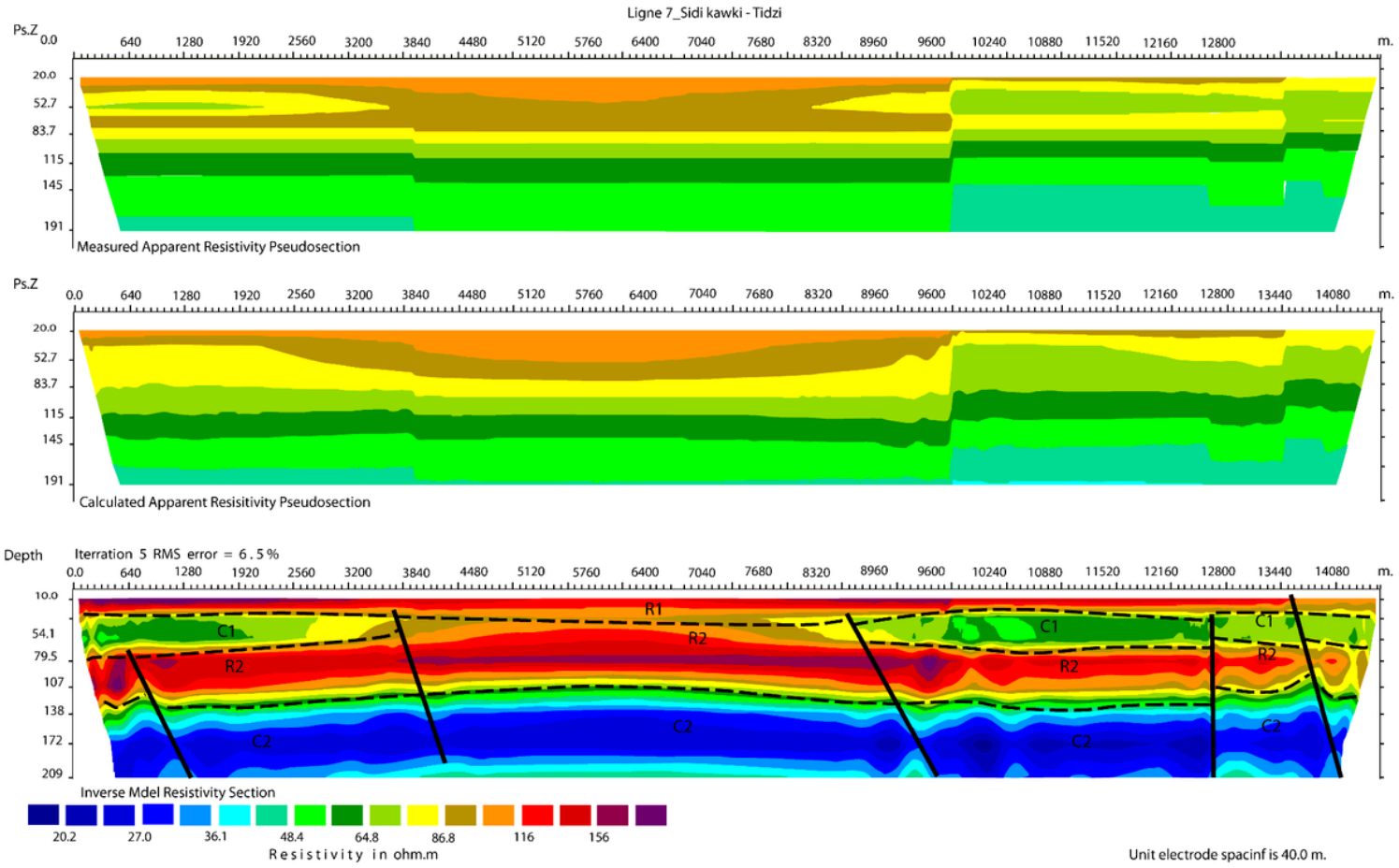

Figure 16

2D electrical imaging section of tomographic line 7 (Sidi Kawki – Tidzi region).

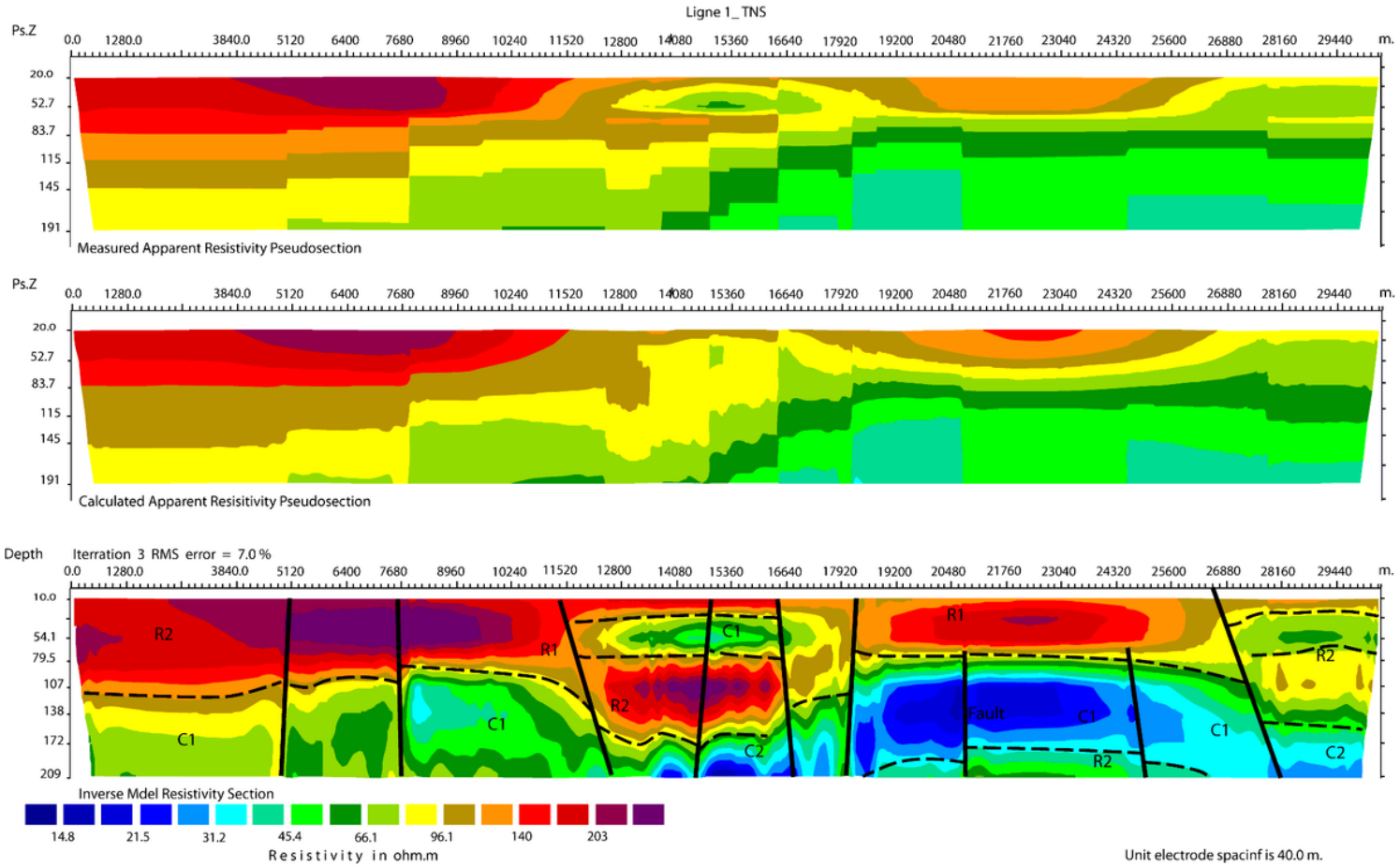

Figure 17

2D electrical imaging section of the North-South tomographic line NS (Agadir Chicht – Tidzi region).